NIST-GCR-94-638

TURBULENT UPWARD FLAME SPREAD ON A VERTICAL WALL UNDER EXTERNAL RADIATION

A. K. Kulkarni, E. Brehob, S. Manohar, and R. Nair
Department of Mechanical Engineering
The Pennsylvania State University
University Park, PA 16802

Issued June 1994
February 1994

Sponsored by:
U.S. Department of Commerce
Ronald H. Brown, *Secretary*
Technology Administration
Mary L. Good, *Under Secretary for Technology*
National Institute of Standards and Technology
Arati Prabhakar, *Director*

Notice

This report was prepared for the Building and Fire Research Laboratory of the National Institute of Standards and Technology under grant number 60NANB8D0849. The statements and conclusions contained in this report are those of the authors and do not necessarily reflect the views of the National Institute of Standards and Technology or the Building and Fire Research Laboratory.

Annual Report
for the period September 30, 1991 to January 15, 1993
on Grant No. 60NANB8D0849

TURBULENT UPWARD FLAME SPREAD ON A VERTICAL WALL UNDER EXTERNAL RADIATION

by

Anil K. Kulkarni, Principal Investigator
Ellen Brehob, Ph.D. Student
Shailesh Manohar, M. S. Student
Rajesh Nair, M. S. Student

Department of Mechanical Engineering
The Pennsylvania State University
University Park, PA 16802

Submitted to
Building and Fire Research Laboratory
National Institute of Standards and Technology
Gaithersburg, MD 20899

ABSTRACT

Progress made on NIST grant number 60NANB8D0849 for the period September 30, 1991 to January 15, 1993 is reported. The overall objective is to understand the upward flame spread phenomenon under simulated surrounding fire conditions by establishing a data base for upward flame spread under external radiation, developing a mathematical model, measuring the relevant basic material properties needed, and checking the validity of the model by comparing its results with data. Emphasis is placed on studying and predicting the behavior of practical wall materials used in building and vehicle interiors, and textiles. In the past year, we measured flame spread on several different materials under a range of external radiant fluxes of up to 15 kW/m^2. A model for describing the upward flame spread process was developed and numerical results were compared with data. The model needed input of certain properties, such as the burning rate characteristics and surface radiation properties. A series of supporting studies were undertaken which provided the needed input properties to the model and other useful material property data. These studies included transient mass loss rate experiments, in-depth radiation absorption analysis and experiments, and reflectance measurements using a specially designed heated cavity reflectometer. Experimental data, appropriately validated model, and radiative properties of materials obtained here should be very useful in fire hazard codes for single or multiple enclosures, as well as for assessing material flammability in a relevant orientation.

TABLE OF CONTENTS

EXECUTIVE SUMMARY

This annual report describes progress made during the period Septembers 30, 1991 to January 15, 1993 on the project Upward Flame Spread on a Vertical Wall Under External Radiation, supported under grant number 60NANB8D0849. The progress is reported for the second year of the project, which is currently being continued in the third year.

The importance of upward flame spread stems from its ability to spread rapidly and presents a significant fire hazard. In post-flashover rooms, the radiant flux levels may reach 100 kW/m^2; but even in pre-flashover enclosure fires, signifi... amounts of energy is irradiated by the fire to the other walls which are yet to burn. It has been observed that certain materials which do not sustain upward flame spread in the absence of external radiation flux (for example, wood), allow the flame to spread when assisted by an external radiation source. Also, it is expected that materials which normally exhibit upward flame spread will have a significant enhancement in flame spread and fire growth in the presence of external radiation. Some of the standard tests such as ASTM E 162 for horizontal flame spread and ASTM E 648 for downward flame spread have indicated that materials which are normally considered safe may exhibit an unacceptable behavior under a real fire situation. No standard test method for ranking materials based on their performance during upward flame spread with external radiation is available, primarily because of the lack of fundamental knowledge in this area.

External radiation affects upward flame spread in two ways. Ahead of the pyrolysis front, the radiant heat flux adds to the heat feedback from the flame and causes the yet-unburned surface of the sample to heat up to the pyrolysis temperature quicker. Behind the pyrolysis front, where the surface area that is already burning, the external radiation increases the mass loss rate of the sample which in turn causes larger flames and enhanced heat feedback to the surface. Both of these effects of external radiation accelerate the upward flame spread.

The present program was undertaken to provide basic understanding of upward flame spread with applied external radiation. It will be extremely useful in improving our capabilities of predicting fire growth in compartments and buildings, and in devising appropriate test methods for wall materials.

The overall project was divided into five tasks. Specific accomplishments made in the past year on each of the tasks are :

(a) Tested several wall materials in our facility for upward flame spread under external radiation,

(b) Formulated a mathematical model for the flame spread process, obtained numerical results, and made comparisons with data for some materials,

(c) Measured local, transient mass loss rate of samples under a range of external radiation flux for several materials,

(d) Measured in-depth radiation absorption properties, and analyzed the absorption characteristics using a 14 band radiation model, for clear and blackened PMMA,

(e) Completed fabrication of a heated cavity reflectometer and measured the spectral hemispherical reflectance of several samples.

Details on the individual tasks accomplished are given in the following sections labeled A through E. Activities related to publications, presentations, and theses related to the grant in the past year are summarized below.

Kulkarni, A. K., C. I. Kim and C. H. Kuo. Turbulent Upward Flame Spread on a Vertical Wall Under External Radiation, Annual Report to NIST, May 1992.

Brehob, E. and A. K. Kulkarni, Measurement of Transient Local Mass Loss Rate of Masonite Under External Radiation, Proceedings of the Fall Technical Meeting of the Eastern Section of The Combustion Institute, pp. 96.1-96.4, October 14-16, Ithaca, NY, 1991.

Manohar, S. S., A. K. Kulkarni, and S. T. Thynell. In-Depth Radiation Properties of PMMA Before and After Surface Pyrolysis, Proceedings of the Fall Technical Meeting of the Eastern Section of The Combustion Institute, pp. 95.1-95.4, October 14-16, Ithaca, NY, 1991.

Manohar, S. S., A. Kulkarni, and S. T. Thynell. Role of In-Depth Absorption in Flame Spread Under External Radiation Over Semitransparent Materials, presented at the Annual Conference on Fire Research, Rockville, MD, October 1992.

Brehob E. G. and A. K. Kulkarni, Experiments on Turbulent Upward Flame Spread Under External Radiation, presented at the Annual Conference on Fire Research, Rockville, MD, October 1992.

Kulkarni, A. K. and S. J. Neches, Simulation of Liquid Spray Atomization in Supercritical Environment Using Various Surface Tension Models submitted to International Conference on Liquid Atomization and Spray Systems, 1993.

Manohar, S. S., A. K. Kulkarni, and S. T. Thynell. In-Depth Absorption of Externally Incident Radiation in Nongray Media, to be presented and published in the proceedings of the 1993 ASME National Heat Transfer Conference, Atlanta, August 1993.

Brehob, E. G. and Kulkarni, A. K., Experimental Measurements of Upward Flame Spread with External Radiation, submitted to the First ISHMT/ASME (US-India) Joint Heat and Mass Transfer Conference, January 1994.

Brehob, E. G. and A. K. Kulkarni, Time-dependent Mass Loss Rate Behavior of Wall Materials Under External Radiation, Fire and Materials, (accepted for publication).

Kulkarni, A. K. and F. Murphy. Interaction of Buoyant Plumes with Two-Layer Stably Stratified Media, Experimental Thermal and Fluid Science (to be published).

Manohar, S. S., A. K. Kulkarni, and S. T. Thynell. In-Depth Absorption of Externally Incident Radiation in Nongray Media, Journal Heat Transfer (accepted for publication).

Costa, J. T. and A. K. Kulkarni. A Numerical Model of Buoyant Plumes in Room Fires with Two-Layer Stratified Atmosphere, submitted to Annual Fire Research Conference, Gaithersburg, MD, 1993.

Nair, R., A. K. Kulkarni, and S. T Thynell. Measurement of Spectral Hemispherical Reflectance Properties of Materials, submitted to Annual Fire Research Conference, Gaithersburg, MD, 1993.

Brehob, E. G. and A. K. Kulkarni, A Numerical Model for Upward Flame Spread Under External Radiation, submitted to Annual Fire Research Conference, Gaithersburg, MD, 1993.

Theses:

Brehob, E., Upward Flame Spread on Vertical Walls under External Radiation, Ph.D. Thesis, in progress.

Kim, C. I., Upward Flame Spread on Vertical Walls, Ph. D. Thesis (completed in December 1991).

Manohar, S., In-depth Radiation Absorption in Semitransparent Materials, M. S. Thesis, (completed in August 1992).

Nair, R., Measurement of Spectral Hemispherical Reflectance Using a Heated Cavity Reflectometer, M. S. Thesis, (completed in June 1993).

Costa, J., A Numerical Model of Interaction of a Buoyant Jet with a Two-Layer Stratified Atmosphere in a Room Fire, M. S. Thesis, (completed in June 1993).

A. EXPERIMENTS ON UPWARD FLAME SPREAD

(AKK and Ellen Brehob; help was also provided by J. Bao, Undergraduate Intern)

In this phase of the project, emphasis was placed on obtaining experimental data for upward flame spread with applied external radiation on practical wall materials. In addition to examining the effect of external radiation on flame spread velocity, other parameters such as line burner strength and preheat time were investigated.

Experimental Apparatus

A detailed description of the experimental facility was pr ted in the last year's report, therefore, only a brief account of the apparatus and procedure is given below. A schematic of the upward flame spread facility at Penn State is shown in Figure A1. The sample materials burned in the apparatus are 30 cm wide, 120 cm high, and of various thicknesses. Samples are installed such that the front surface is flush with the larger, outer panel of inert material. On either side of the panel of inert material are water-cooled copper side shields which are angled forward at 45 degrees. A line burner is used to ignite the lower edge of the sample. The burner is fueled with propane, and by varying the flow rate of propane, the line burner strength may be set at values from 3.6 to kW/m. Two electric-powered infrared heating panels are angled towards the sample materia to supply a heat flux which simulates the sample being burned in a room in which other walls are on fire and supplying radiant energy. A maximum average flux of 15.1 kW/m^2 can be supplied to the sample.

A typical test involved turning the radiant panels on until they reached steady-state. During this time, the sample material was shielded from the radiation. Nearly simultaneously the shield was removed and the line burner placed in front of the sample. The burn event was video taped and by reviewing the tape, flame tip height as a function of time was determined. Flame tip is defined as the highest location of continuous luminous flame or the highest location of a luminous flame ball (separated from the continuous flame) larger than 5 cm. In some cases pyrolysis front history (chosen as the location of darkening of the sample surface) was determined from the video tape. Pyrolysis front measurements are based on single frames of the burn event.

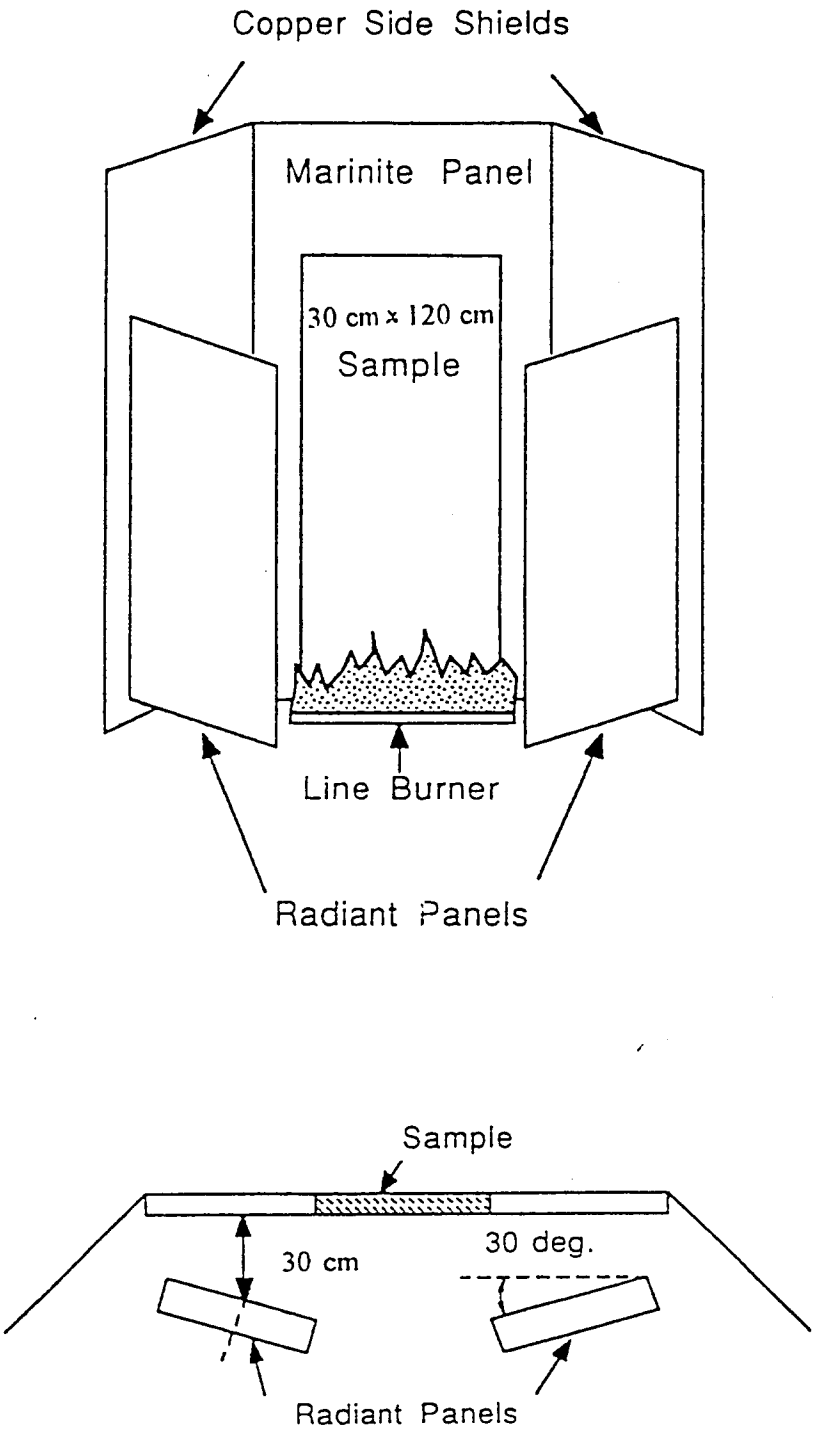

Figure A1: Experimental Upward Flame Spread Apparatus
Front and Top View

Results

Effect of External Radiation: Figure A2 shows flame height versus time data for several materials. All of the plots have the same test conditions, namely, igniter strengths of 18.5 kW/m, external radiation of 7.6 kW/m^2, and no preheat. PMMA (3.2 mm thick) is the only plastic shown in this figure. This material exhibits sustained flame spread without external radiation, but the application of additional heat flux causes a faster rate of flame spread. Without external radiation, the other materials (all others are wood-based or cotton) do not show flame spread to the top of the sample. The flame height data without external radiation is not shown in Figure A2 because the flames do not spread much above the height of the line burner. The plots fall nearly on top of each other and c... ...tter the figure. With external radiation of 7.6 kW/m^2, various trends are seen for the materials: particle board (15.9 mm) and poplar (19.0 mm) show sustained upward flame spread, plywood (12.7 mm) shows an initial period of flame spread but the flames recede before the pyrolysis front reaches the top of the sample, and fire retardant plywood (12.7 mm) and cotton textile show no flame spread. The cotton textile is a relatively thin material, and therefore, the time scale of burning for this sample is much shorter than the other materials.

Flame height as a function of time for 15.9 mm particle board with igniter strength of 18.5 kW/m, no preheat, and various levels of applied external radiation are shown in Figure A3. Pyrolysis front location as a function of time is also plotted to illustrate which tests exhibit sustained upward flame spread. For sustained upward flame spread, the flame front should stay ahead of the pyrolysis front, and the pyrolysis front and flame front should both reach the top of the sample. With external heat fluxes of 7.6 kW/m^2 or greater, the flame and pyrolysis front spread to the top of the sample. This value is similar to the results obtained by Saito et al. (1986) which showed that sustained upward flame spread on particle board did not occur until the critical flux level of 7.0 kW/m^2 had been reached Two plots from previous work (Saito et al., 1986 and Quintiere et al., 1985) are also shown in Figure A3. Again, the igniter strengths and material thicknesses are different between the experiments, but the magnitude of the flame spread is in the same range as the data being presented.

In Figure A4, experimental data for poplar wood is presented. The only test condition varied between these plots is the level of external radiation. Pyrolysis fronts were measured for each of the runs by noting a change in the color of the sample surface. The pyrolysis locations corresponding to the tests run at 2.2 kW/m^2 and 0.5 kW/m^2 are shown in the

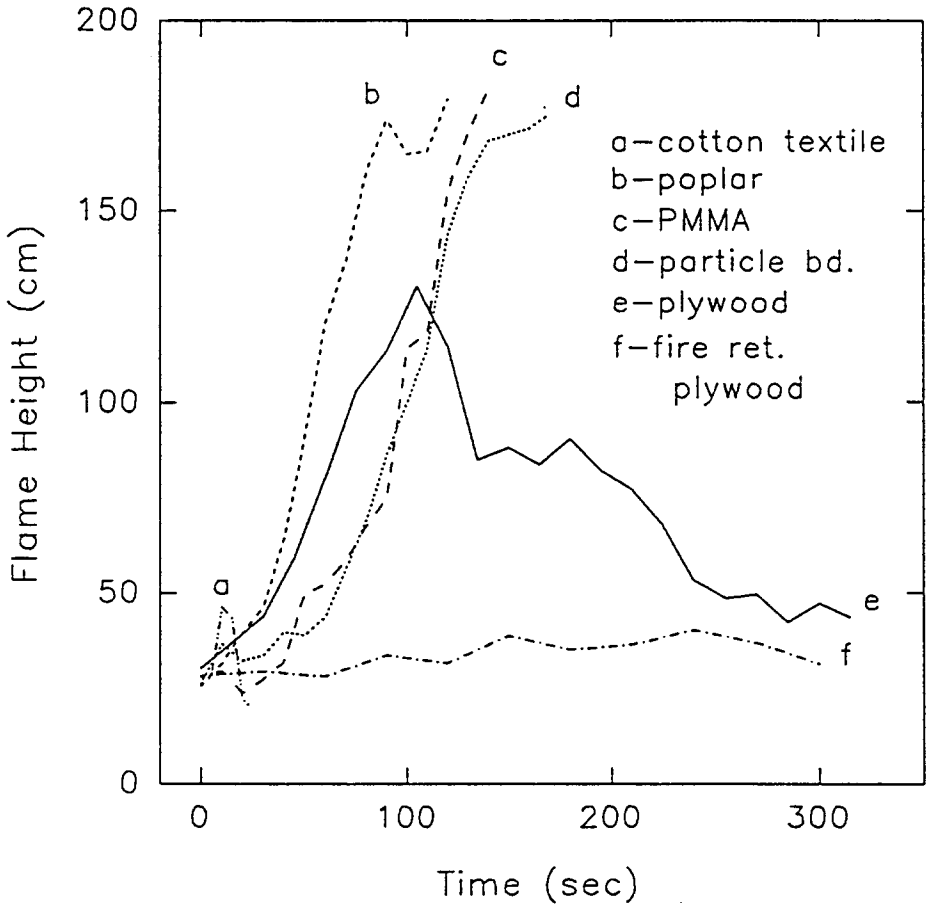

Figure A2: Flame Spread for Various Materials with External Radiation of 7.6 kW/m^2, Igniter at 18.5 kW/m, No preheat

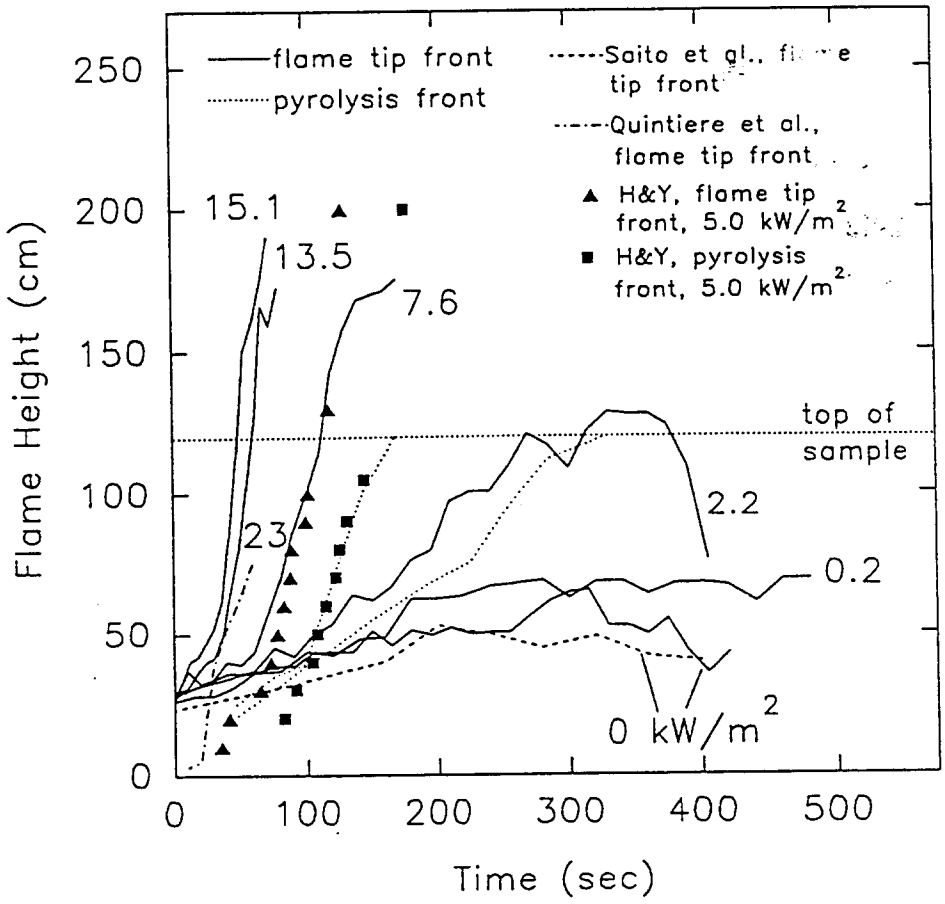

Figure A3: Flame Spread for Particle Board at Various Levels of External Radiation, Igniter at 18.5 kW/m, No preheat

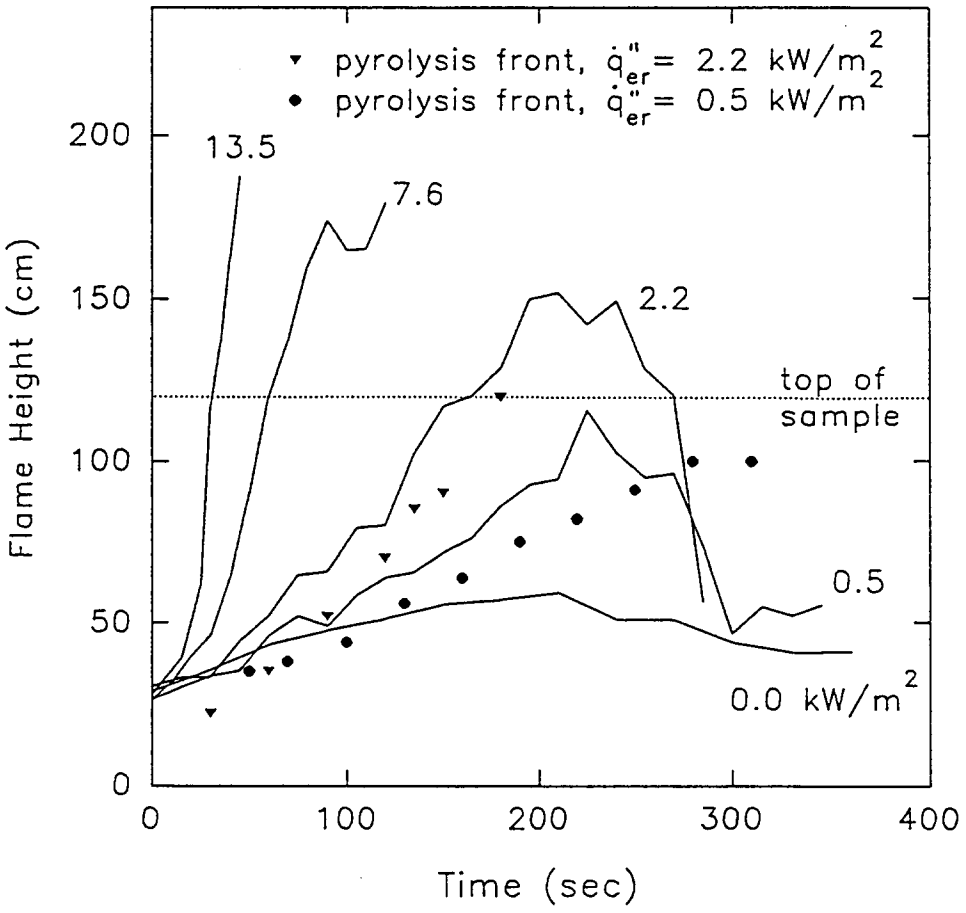

Figure A4: Flame Spread for Poplar at Various Levels of External Radiation, Igniter at 18.5 kW/m, No preheat

figure. For flux levels of 2.2 kW/m^2 and greater, the flame spread is sustained to the top of the sample. This is demonstrated in the figure by the pyrolysis front reaching the top of the sample. (The sample height is denoted in the figure by the dotted line at 120 cm.) Although the flames for the 0.5 kW/m^2 heat flux case reach the top of the sample, the pyrolysis front does not; and eventually the flames recede below the pyrolysis front.

A cotton textile (broad cloth) was tested and the results are shown in Figure A5. At the lowest two levels of external radiation, no upward flame spread occurred. The cloth burned only over the area covered by the line burner flames. At a radiation level of 7.6 kW/m^2, the flames spread part way up the material but died out before reaching the top of the sample. At the highest level of external radiation (13.5 kW/m^2) the flames very quickly moved up the full height of the sample. The pyrolysis front was difficult to measure because the application of the radiant flux caused the material to begin to turn brown (char) over most of the sample simultaneously. Since the material is relatively thin compared to other materials tested, the material was fully consumed and a well defined burnout front was seen. The burnout front location as a function of time is shown in Figure A5 for the sustained flame spread case at 13.5 kW/m^2.

Flame height measurements for plywood are shown in Figure A6. For this material sustained flame spread nearly occurred for 7.6 kW/m^2 and was definitely sustained for external radiation of 13.5 kW/m^2 and above. Data from Hasemi et al. (1990) is also shown in the figure and shows sustained flame spread for external radiation of 5.0 kW/m^2. With a sample height of 200 cm, the flame tip front and pyrolysis front reached higher levels than the present work which has a sample height of 120 cm. In addition to the effect of external radiant flux, some of the differences between the data may be attributed to test parameters such as the igniter strength and preheat time which were not identical between sets of data from different investigators. Preheating of the sample tested by Hasemi et al. may result in a lower level of heat flux being required for sustained flame spread. Above the critical flux level, the higher levels of external radiation caused faster upward flame spread.

In sustained flame spread, an increase in pyrolysis front velocity corresponds to an increase in the flame tip velocity. The trend of increased velocity of pyrolysis front and flame tip front due to increased external radiation is supported by the experimental data presented above. Several other test parameters were varied to determine their effect on the flame spread rate.

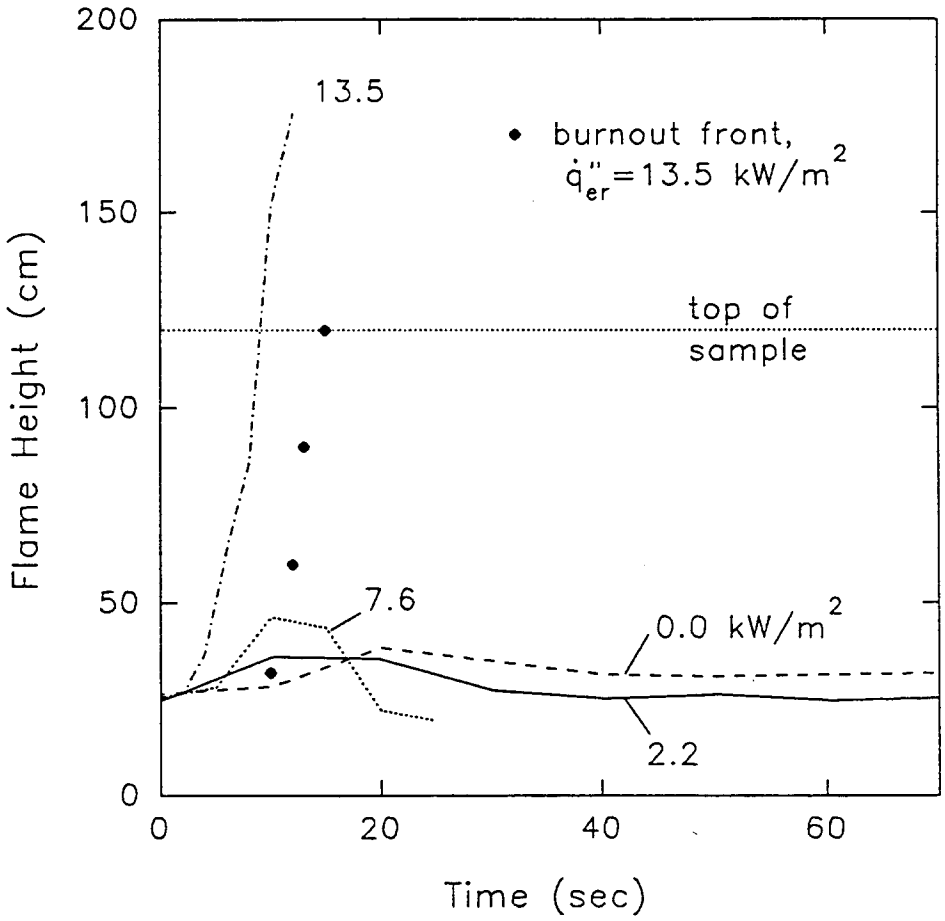

Figure A5: Flame Spread for Cotton Textile at Various Levels of External Radiation, Igniter at 18.5 kW/m, No preheat

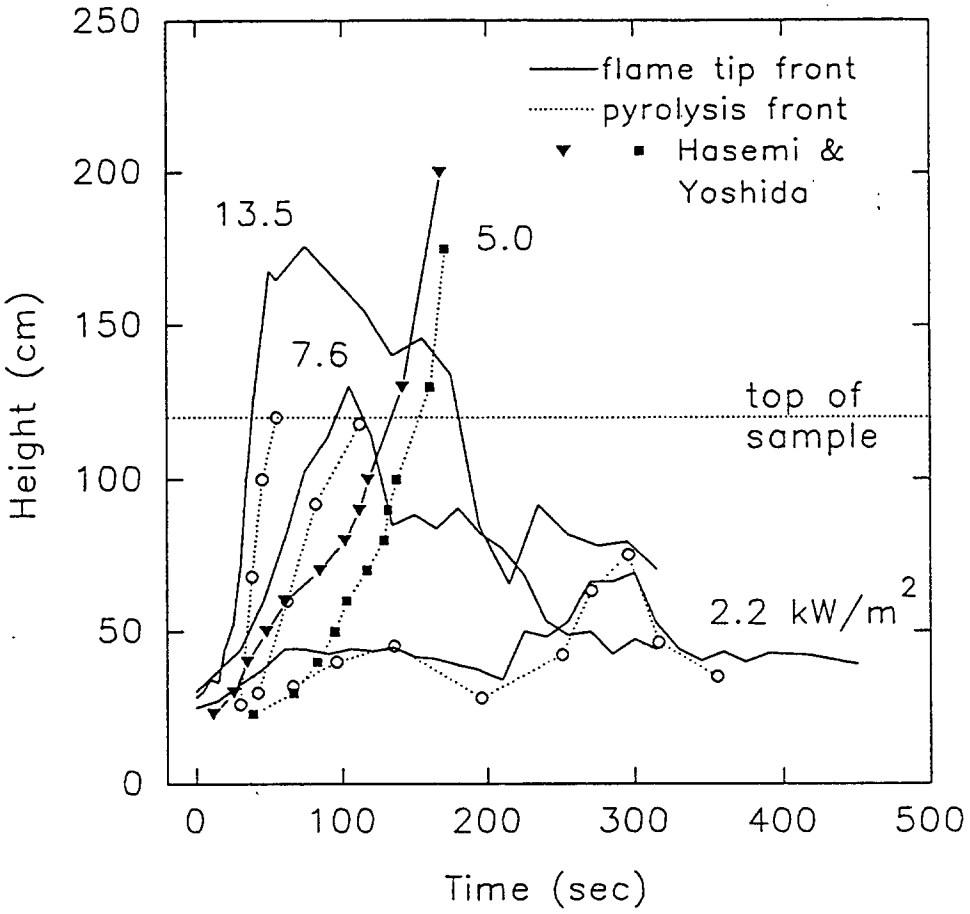

Figure A6: Flame Spread for Plywood at Various Levels of External Radiation, Igniter at 18.5 kW/m, No preheat

Effect of Igniter Strength: In order to examine the effect of igniter strength on upward flame spread, the level of external radiation was held constant at 2.2 kW/m^2 for particle board samples with no preheat. Three levels of igniter strength were used; 3.6 kW/m (results in a flame height of 10 cm), 11.0 kW/m, and 18.5 kW/m (results in a flame height of 30 cm). In Figure A7, it can be seen that higher levels of igniter strength caused the flames to spread higher, but did not result in sustained flame spread. The igniter strength is only a factor in the initial phase of flame spread, but eventually the flames spread activity moves out of the region over which the igniter has any influence. Steady-state flame spread would not be expected to show any effect due to igniter strength.

Effect of Preheat: In Figure A8, the effect of preheating particle board samples prior to ignition was examined. The preheated sample was exposed to a radiant flux of 2.2 kW/m^2 until the temperatures (measured using thermocouples installed on the front and back surfaces of the sample) were nearly constant. The average temperatures of the front and back surfaces were 142 C and 76 C, respectively. Once steady-state conditions were reached, the sample was ignited. The non-preheated sample had a temperature of 42 C when it was ignited. Enough energy must be supplied to the sample to heat the surface up to the pyrolysis temperature (about 350 C for particle board). Preheating the sample raised the surface temperature by 100 C, and therefore less time and/or energy was needed to get the surface to the temperature required for pyrolysis to begin. The preheated sample shows significantly faster flame spread than the sample which was shielded prior to ignition. A theoretical estimate of the effect of preheat on the steady-state spread rate of the pyrolysis front (equation presented above) shows the same trend as that seen in the experimental work.

Effect of Sample Thickness: In Figure A9, flame spread for several thicknesses of particle board (9.5 mm, 15.9 mm, and 25.4 mm) are shown. The particle board thickness used in all previous tests was 15.9 mm. The flame spread without external radiation (not shown in the figure) is the same for all three thicknesses. With the application of 2.2 kW/m^2 of external radiation, the flame spread is slightly higher for the thinner materials, but no significant changes in flame spread rate may be associated with the sample thickness. Thermocouple measurements of the back surface temperatures for all three samples showed very little change from the ambient temperature over the time period of the burn event. Many common materials thicker than 1 mm may be assumed thermally thick (Quintiere, 1985) for the length of time typically associated with upward flame spread. Therefore, the

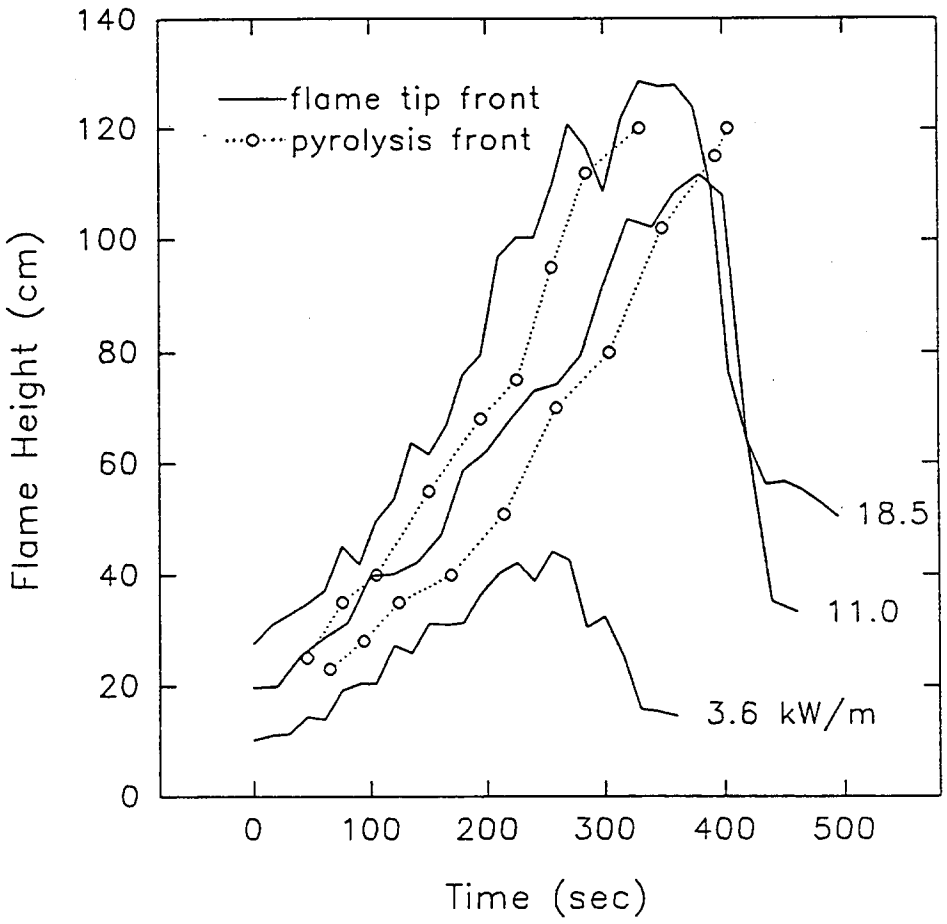

Figure A7: Effect of Igniter Strength on Flame Spread, Particle Board, External Radiation of 2.2 kW/m^2, No preheat

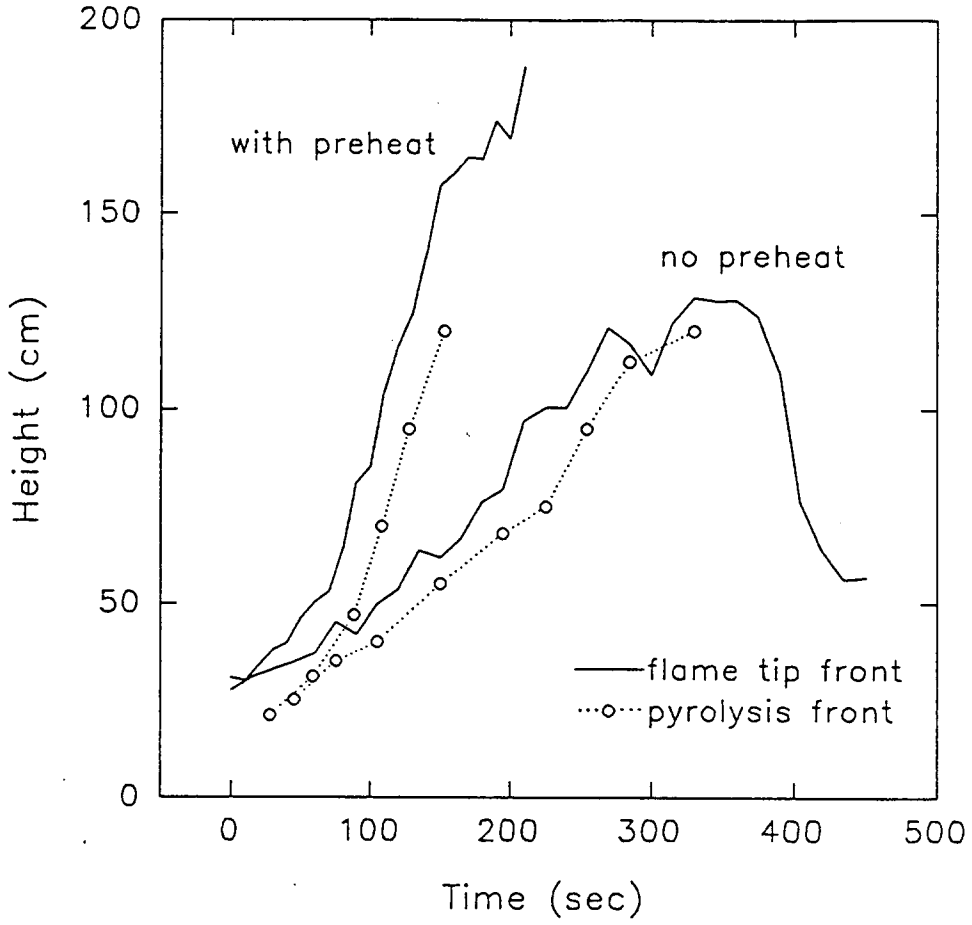

Figure A8: Effect of Preheat on Flame Spread,
Particle Board, External Radiation of 2.2 kW/m^2, Igniter at 18.5 kW/m

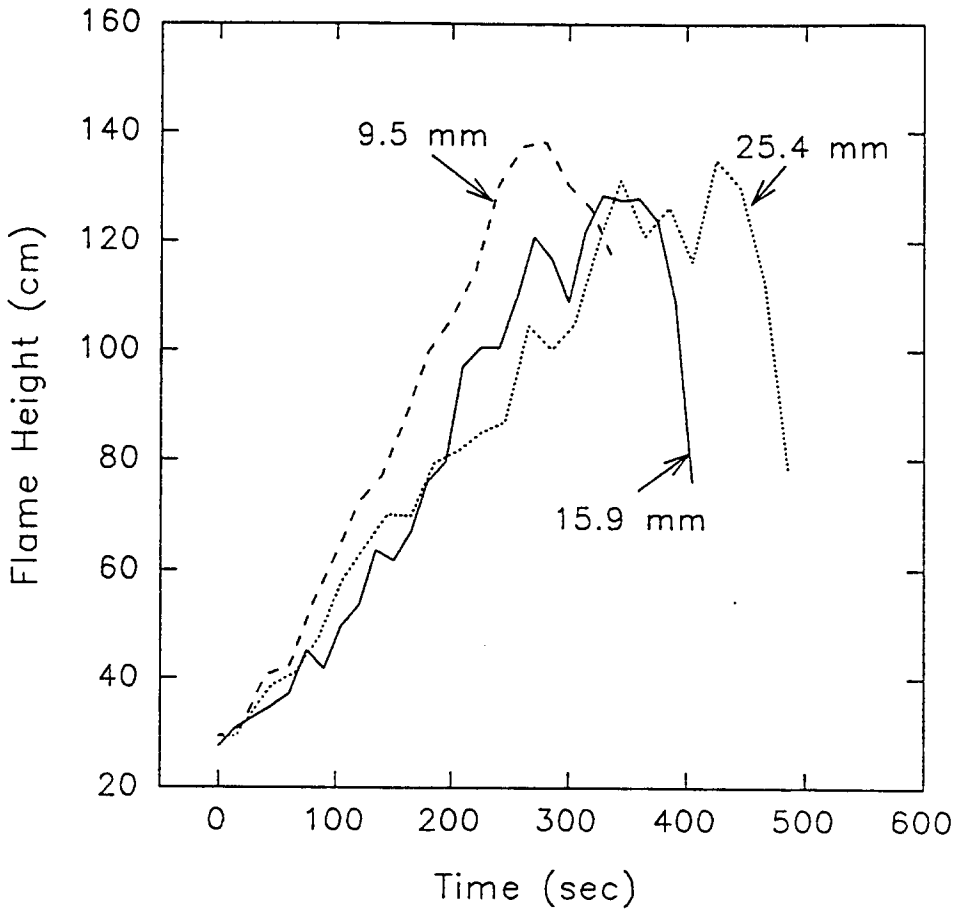

Figure A9: Effect of Thickness on Flame Spread on Particle Board, External Radiation of 2.2 kW/m^2, Igniter at 18.5 kW/m, No preheat

equation for pyrolysis front velocity is not a function of material thickness, and the experimental data supports this result.

Summary and Conclusions

Experimental measurement of flame spread with external radiation was made for various materials. Flame height, temperature on the front and back surfaces, and heat feedback to front face were recorded as a function of time for 120 cm by 30 cm samples. Infrared heating panels were used to supply radiant fluxes of up to 15 kW/m^2 to the sample. Many wood-based materials did not exhibit flame spread to the top of the sample when ignited and without applied external flux. With moderate levels of external radiation (5-10 kW/m^2), many of these materials did have sustained flame spread to the top of the sample. Also, with increasing external radiation levels, the flames spread was more rapid. A comprehensive series of tests was run on particle board to investigate the effect of igniter strength, preheat of the sample, and sample thickness. The igniter strength was not a significant factor and did not cause the flame spread to be sustained; but the effect of preheat, even at moderate levels of radiant flux, was important and did cause sustained flame spread. The effect of sample thickness did not significantly alter upward flame spread rates. Experimental data obtained in this project will be used to aid in the development of a numerical flame spread model and then to validate the model.

References

Saito, K., J. G. Quintiere, and F. A. Williams, 1986, *Fire Safety Science Proceedings from the First International Symposium*, p. 75-86.

Quintiere, J. G., M. Harkleroad, and Y. Hasemi, 1985, AIAA paper no. 85-0456, p. 1-16.

Hasemi Y. and M. Yoshida, 1990, U.S.-Japan Cooperative Wall Fire Experiment and Related Projects, First Interim and Internal Report, October.

B. ANALYTICAL MODEL AND COMPARISONS WITH DATA

(AKK and Ellen Brehob; based on the work of C. I. Kim, a former graduate student)

Development of the Model

The physical system under consideration is depicted in Figure B1. A vertical combustible wall with infinite width is ignited at the bottom. When making computations for comparison with data, the sample is assumed to be 1.2 m high to simulate the geometry in the experimental setup. A line burner supplied with natural gas having a typical strength of 18 kW/m is placed at the bottom of the vertical wall sample. Because of the heat flux provided by the radiation panels and the flames of the burner, the surface temperature of the bottom section of the wall rises until it reaches a certain characteristic temperature, T_{ig}, at which time the material starts pyrolyzing significantly. Then, flames from the burning of pyrolyzed fuel cover the solid fuel above the pyrolysis front (x_p), which is heated by the energy feedback, $\dot{q}''_w(x,t)$, from the flames. The heat feedback consists of both the flame heat feedback and external radiation. When unburnt fuel heats up to T_{ig}, it starts pyrolyzing, the flames grow taller, and thus, the process of upward flame spread is continued. The important parameters and processes contributing to the upward flame spread, therefore, are the local mass loss rate of the wall on the pyrolyzing surface, $\dot{m}''$, the flame tip height, x_f, the heat feedback from the flames to the unburnt wall surface, $\dot{q}''_w$, and the heating of the unburnt fuel above pyrolysis edge.

The model for describing the upward flame spread process is developed in four major parts:

(i) *Heating of the yet-unpyrolyzed section of the wall* : It is well established that the flame spread process depends on how fast the unburnt fuel ahead of the pyrolysis front can be heated to a critical temperature (or a range of temperatures) that causes significant pyrolysis. The surface temperature as well as the inner temperature of the two-dimensional vertical wall, initially at the temperature of T_o, are obtained by solving transient two-dimensional heat conduction equation with transient boundary conditions,

$$\frac{\partial^2 T}{\partial x^2} + \frac{\partial^2 T}{\partial y^2} = \frac{1}{\alpha}\frac{\partial T}{\partial t} \qquad (1)$$

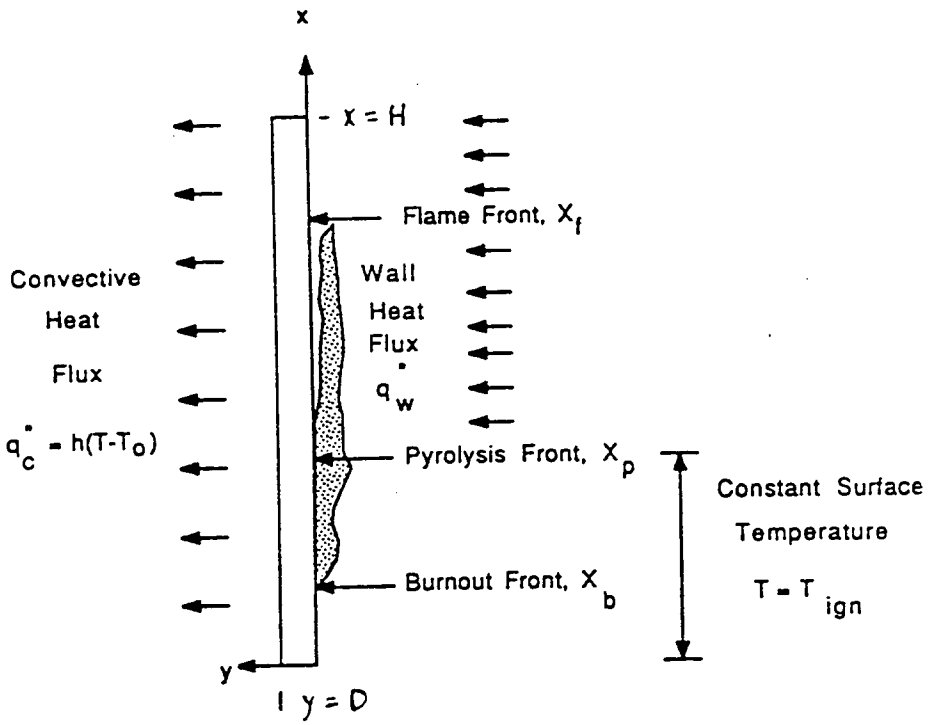

Figure B1: Boundary Conditions for the Burning Wall

Initial Condition: $T(x,y,0) = T_o$

Boundary Conditions: $T(x,0,t) = T_{ign}$ for $x < x_p$

$$-k\left|\frac{\partial T}{\partial y}\right|_{y=0} = \dot{q}''_w(x,t) \quad \text{for } x > x_p$$

$$-k\left|\frac{\partial T}{\partial y}\right|_{y=D} = h(T-T_o)$$

$$-k\left|\frac{\partial T}{\partial x}\right|_{x=0} = -k\left|\frac{\partial T}{\partial x}\right|_{x=H} = 0$$

where $y = 0$ to D and $x = 0$ to H represents the domain for calculations. The thermal conductivity k is an average value for the material. (In general, k can take different constant values for laminated or composite materials. In the present work, a single value reported in literature is used for the materials studied.) With the time-dependent boundary conditions, use of one-dimensional or two-dimensional conduction requires about the same computation time. The 2-D equation is preferred because it gives slightly better accuracy (especially around the pyrolysis edge area where there is temperature gradient in the x direction), and easier definition of computation domain. It is assumed that the ignition temperature does not vary with location, the material is inert during the heating process, and the heat loss to the back side of the wall is in the form of convection to the ambient atmosphere.

The forward heat flux, $\dot{q}''_w(x,t)$, is perhaps the most important parameter in the flame spread model, which is discussed below.

(ii) *Forward heat flux*, $\dot{q}''_w(x,t)$: This is the heat feedback to the wall above the pyrolysis front and it is responsible for raising the surface temperature to some critical value which causes significant pyrolysis (typically assumed to be ignition temperature). As a first approximation, $\dot{q}''_w(x,t)$ has been assumed to be constant equal to 25 kW/m^2 up to a certain height and then zero above in the absence of external radiation. (Delichatsios, 1991) Analytical derivation of $\dot{q}''_w(x,t)$ involves use of several measured properties in order to estimate the heat flux for a given material, which are often not available, or the available properties are not sufficiently accurately known. Therefore, in the present work, a generalized form of $\dot{q}''_w(x,t)$ is obtained from *measured* data in order to allow adequate representation of $\dot{q}''_w(x,t)$.

The effect of external radiation comes into play in modeling of the forward wall heat flux term. It is modeled as,

$$\dot{q}''_w(x,t) = \dot{q}''_{wo}\exp\left[C_o\left(\frac{x-x_p}{x_f-x_p}\right)\right] + \dot{q}''_{er} - \dot{q}''_{rerad} \qquad (2)$$

where $\dot{q}''_{wo}$ is the heat feedback from flames to surface just above $x = x_p$, the pyrolysis height. In our previous study (Kim, 1991) values of $\dot{q}''_{wo}$ for various materials were obtained by curve-fitting the heat feedback data (obtained in the absence of external heat flux) and extending the curve to $x = x_p$; these values are listed in Table 1. The above correlation allows determination of $\dot{q}''_w(x,t)$ based on a single value of $\dot{q}''_{wo}$ which may be treated as a "fire property" of the wall material.

Table 1. Maximum forward heat flux.

Material	Maximum Forward Heat Flux, $\dot{q}''_{wo}$ (kW/m^2)
Black PMMA	31.9
Clear PMMA	34.6
Cardboard	34.5
Douglas-Fir Particle Board	24.3
Rigid Polyurethane Foam	18.8
Carpet	25.6

The decay factor C is determined as – 1.37. The above equation for forward heat flux requires flame height, x_f, which is discussed below.

(iii) *Instantaneous flame height* : The flame size depends on the cumulative flame energy release rate based on the integration of local burning rate over the entire pyrolyzing region on the wall. The larger the total energy release rate, the taller are the flames, and a greater area ahead of the pyrolysis front is preheated. The flame tip height is obtained from an available correlation (Saito et al., 1986)

$$x_f(t) - x_b(t) = K\left[\dot{Q}'(t) + h_c\int_{x_b(t)}^{x_p(t)} \dot{m}''\, dx\right]^n \qquad (3)$$

where the bracket represents the total energy release rate in the fire which is the sum of the energy release rate by the igniter ($\dot{Q}'$, in kW/m) and the energy released due to pyrolyzing surface, h_C is the heat of combustion of the fuel, and K and n are experimentally obtained constants. Experimental correlation factors K and n were determined as 0.433 and 2/3 respectively (Orloff et al., 1975)

The above equation for flame height needs the estimate of the total energy release rate, which is obtained as shown below.

(iv) *The local mass loss or burning rate*, $\dot{m}''(t)$: The total energy release rate at any instant is obtained from the total mass loss rate of the burning slab multiplied by the average heat of combustion of pyrolyzed fuel. The total or cumulative mass loss rate is calculated by integrating the local mass loss rate over the entire burning area. From the flame spread point of view, the history of local burning rate is a characteristic of the combustion behavior of the material and it depends on the physical, chemical and geometric properties of the wall material. For a slab of a homogeneous material like PMMA, the rate of burning increases in the beginning because the heat losses to the interior decrease initially, goes through a maximum burning rate, and finally drops to zero due to heat loss from the back side of finite thickness samples (Kulkarni and Kim, 1990). Even with a constant heat input, the mass loss rate is not constant for most materials. In case of a wood panel, for example, there may be an initial peak due to volatile gases followed by slow burning of char. In the simplest form, $\dot{m}''$ has been assumed to be constant until all the combustible mass is pyrolyzed; other forms have employed inverse square root or exponentially decreasing dependence. (Saito et al., 1986 and Delichatsios, 1991). During the flame spread process *different vertical locations are at different stages of burning*, for example, the region near the leading edge may be close to burnout, the region further up may be burning at the peak rate, and the pyrolysis edge is at the just-ignited state. The history of burning is, therefore, very important in the flame spread process.

It is assumed in the present model that the mass loss rate history at each location is the same once ignition occurs, irrespective of the location on the vertical wall. Such an assumption has been made before and found useful. (Saito et al., 1986). These local mass loss rate functions are used in the present calculations. In the present work local mass loss

rate functions are obtained from separate small scale mass loss rate experiments, which are described in detail in section C.

To close the upward flame spread model, a consideration of pyrolysis height (x_p) and burn-out edge (x_b) is necessary. The definitions for these parameters are given by

$$x_p = x \text{ when } T_{surface}(x) = T_{ign} \tag{4}$$

$$x_b(t) = x_p(t-t_b) \tag{5}$$

where t_b is the burn-out time (the amount of time between when a particular element first reaches pyrolysis temperature until the combustible part of material has been consumed).

Equations (1) through (5) form a complete set of equations with appropriate boundary conditions. The general solution procedure is as follows: at any given instant, t, first the local burning rate, $\dot{m}''$, is computed; it is then integrated over $x = x_b$ to $x = x_p$; then the total heat release rate, flame height, and $\dot{q}''_w(x,t)$ are computed; then the temperature distribution in the solid is computed to obtain the surface temperature distribution; finally the new x_p is determined based on the condition $T = T_{ig}$ at the surface. The computation is started at the instant the burner is placed near the bottom of the wall. Equations are solved using a finite difference numerical procedure. Due to stiff temperature gradients close to the surface, a nonuniform grid is used with a higher grid density near the surface.

Comparisons with Data

Some preliminary results of the numerical model have been made for 3.2 thick mm hardboard and are shown in Figure B2. Flame height and pyrolysis front histories at two levels of external radiation are compared in the figure. The convergence of the flame and pyrolysis height for the unradiated case is indicative of extinguishment of the upward flame spread prior to reaching the top of the sample. The experimental measurement for hardboard also confirmed this result. For the case with an average external flux of 2.2 kW/m^2 applied, the flame and pyrolysis front spread is faster and the sample sustained flame spread to the top. Further work on comparison of predicted data with experimental results and predictions for other materials is in progress.

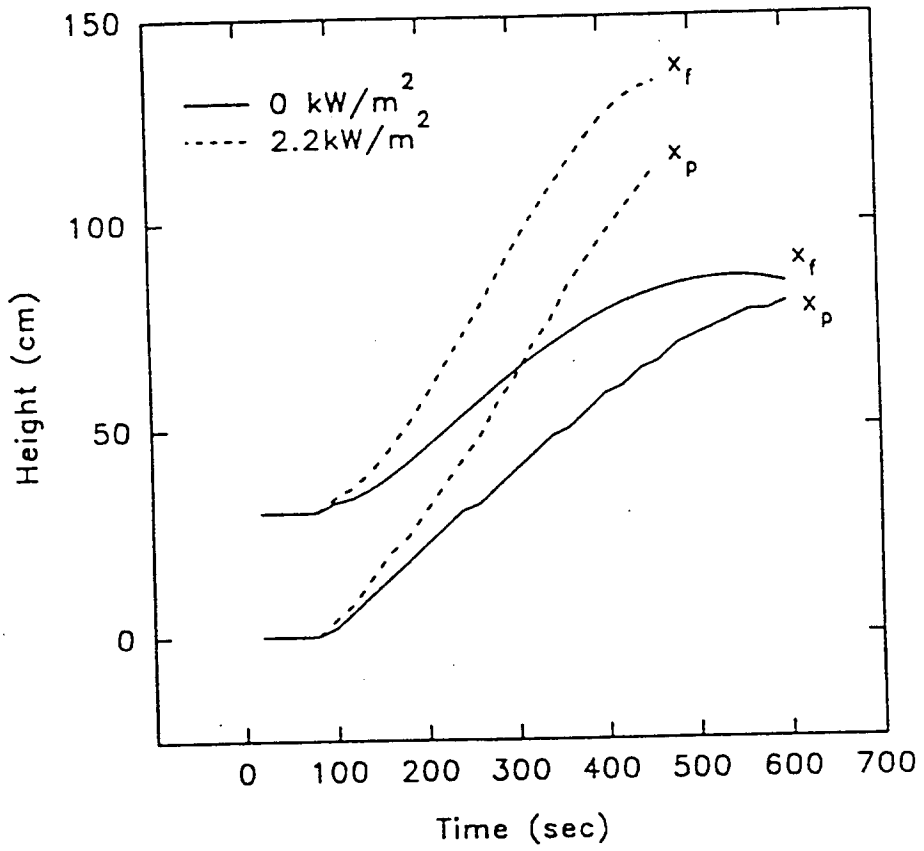

Figure B2: Flame Height and Pyrolysis Front Histories for 3.2 mm Hardboard at Two Levels of External Radiation

References

Delichatsios, M. M., Mathews, M. K., and Delichatsios, M. A., 1991, An Upward Fire Spread and Growth Simulation, *Fire Safety Science-Proceedings from the Third International Symposium*, Hemisphere Publishing, p. 207-226.

Kim, C. I., 1991, Upward Flame Spread on a Vertical Wall, Ph.D. Thesis at the Pennsylvania State University, University Park, PA.

Kulkarni, A. K. and C. I. Kim, 1990, Heat Loss to the Interior of a Free Burning Vertical Wall and Its Influence on Estimation of Effective Heat of Gasification, *Combustion Science and Technology*, Vol. 73, pp. 493-504.

Orloff, L., deRis, J., and Markstein, G. H., 1975, Upward Turbulent Fire Spread and Burning of Fuel Surfaces", *Fifteenth Symposium (International) on Combustion*, The Combustion Institute, Pittsburgh, PA, p. 183-192.

Saito, K., Williams, F. A., and Quintiere, J. G., 1986, Upward Turbulent Flame Spread, *Fire Safety Science Proceedings of the First International Symposium*, Hemisphere Publishing, p. 75-86.

C. MASS LOSS RATE EXPERIMENTS

(AKK and Ellen Brehob)

As explained earlier, local mass loss rate is an important input in our flame spread model. One of the effects of external radiation is to cause increased mass loss rate of the fuel, which produces larger flames. In the present work, $\dot{m}''(t)$ is obtained using a simple but specially designed small scale apparatus. The specific objectives of the present work were to: 1) measure mass loss as a function of time which will be a unique characteristic of the material or combination of materials making up the wall, 2) identify important time constants and "fire properties" for each material which may be useful in characterizing material flammability, and 3) obtain data which can be put in a suitable analytical form for use in numerical models.

Results for hardboard (trade name Masonite) were presented in the last year's report. Further review of those results and suggestions by others revealed a somewhat better approach for presenting the data. In this report, results are presented for polymethylmethacrylate (PMMA) and cardboard; results of hardboard are included for completeness. Background and the description of apparatus are also presented in brief. Additional details on this task may be found in Brehob and Kulkarni (1993).

Background

In many enclosure and corridor fires, the radiation from surrounding walls has a significant effect on fire growth and the spread rate of flames. Levels of radiant flux in the range of 20 to 100 kW/m^2 are commonly found in post-flashover enclosure fires (Babrauskas, 1991). If a wall exposed to a high level of external radiation is ignited at the bottom, one of the effects of the external heat flux is the enhanced burning rate of the ignited area, which causes larger flames and faster upward flame spread (Fernandez-Pello, 1977). As described in the previous section, models for predicting flame spread on burning surfaces need an accurate input of transient heat release rate at each location on the wall.

Smith and Green (1987) designed a mathematical model for a developing fire in a compartment which required experimental heat release data. For their model, the heat release rate was correlated with the total heat released. The use of experimental data is encouraged

by the authors, as the use of a few fundamental constants to express the heat release rate is presumed to be a long way off. The local mass loss rate is an input parameter for several numerical and theoretical models. In the work by Cleary and Quintiere (1991), a model for predicting flame spread in various orientations is developed in terms of "fire properties" of a material which are measurable in small-scale experiments. One of the required properties is an average peak heat release rate which is calculated from the transient heat release rate over the burnout time. The Karlsson and Magnusson (1991) model for simulating room fires requires an analytical approximation of the heat release rate as a function of time. Kulkarni et al.. (1991) investigated the transient local mass loss rate of vertical burning slabs of PMMA with no external radiation flux by comparing an experimental measurement with a theoretical prediction. For the non-charring material tested, the agreement in the mass loss rates was good. Mitler (1990) used both a mass loss rate based on a steady-state energy balance at the surface and one from experimental measurements in his model to predict pyrolysis front position with time. For a non-charring, non-melting material, the two mass loss rates yielded similar results, but the author suggested that the experimentally measured mass loss rate has the advantage of accounting for material thickness and charring.

Previous work has demonstrated a need for accurate HRR information and various methods to obtain this information have been employed. The burning intensity of plastics and wood samples was measured by Tewarson and Pion. (1976). for samples in a horizontal configuration. Transient mass loss rates for particle board and PMMA under external radiation have been measured by Vovelle et al. (1984). In their experiments, samples were pyrolyzed in a vertical orientation but no ignition flame was supplied. They found that the mass loss rates for PMMA, when properly scaled with radiant flux, tended to collapse onto the same curve. For a charring material such as particle board, additional terms which give information on the density profile of the material must be included to obtain similar curves. Heat release rate (HRR) which can be related to mass loss rate may also be measured in the Cone Calorimeter (Babrauskas, 1990 and Babrauskas, 1991). In this device, the sample orientation and ignition source location are variable. Another widely used device for measuring heat release rate was designed at Ohio State University, and the OSU device uses a thermopile to measure the temperature of the gases leaving the sample burning chamber (Tran, 1990). In this method the sample orientation, level of external radiation, and location of ignition may be varied. The HRR and other parameters measured in the Cone and the OSU apparatus have been suggested as a means of classifying the flammability of materials.

Experimental Setup

The experimental setup is shown in Fig. C1. The infrared radiant panels can produce a maximum of 63 kW/m^2 of radiant flux and were adjustable to lower levels. The heating elements in the panels reach temperatures of 1088 K (1500 ^oF) and are embedded in a ceramic material and covered with a Corning Vycor face plate. In the current configuration, the panels subjected the sample to a maximum radiant flux of nearly 12 kW/m^2 with a variation of less than 10% of the average heat flux over the exposed sample area. A 120 mm by 120 mm piece of sample material was flush mounted in a panel of inert material and had a backing of the same inert material. The sample and holder were installed on one end of the balance arm. The sample was exposed to flux from the radiant panels and uniformly covered by turbulent flames from a propane line burner. Mass loss of sample was measured continuously by an electronic balance, and the output voltage from the balance was fed to the data acquisition system. (More details of the mass loss apparatus are available in reference 12.) The samples were not preheated prior to ignition. In this set of tests, the radiant panels were preheated for 30 minutes, and during this time the sample material was shielded from the radiant flux. Nearly simultaneously, the radiant energy shield was removed, and the line burner placed in front of the sample.

Data Analysis

The voltage output from the balance was converted to units of mass loss per unit area, smoothed using an error detection routine, and corrected to account for the mass loss of the sample holder. A typical mass loss curve is shown in Fig. C2. Also denoted in the figure are the stages of burning. Mass loss versus time curves for some materials showed an initial preheat time during which no significant mass loss was measured. Following the preheat stage was a flaming combustion stage which exhibited significant mass loss. In the final stage, the glowing combustion stage, the mass loss is fairly small and occurs at a steady rate. The quantities used to characterize the mass loss of a sample were the amount of time required for a given percentage of the consumable mass of the sample to be burned. (The consumable mass of the sample was determined by weighing the sample prior to testing, allowing the sample to fully burn, and then subtracting the weight of the ashes left.) For example, the time for 25 percent of the sample's mass to be consumed may easily determined from the graph of mass loss rate. A quantity used by previous researchers for characterizing the flammability of a material is the peak mass loss rate and the time to the peak mass loss

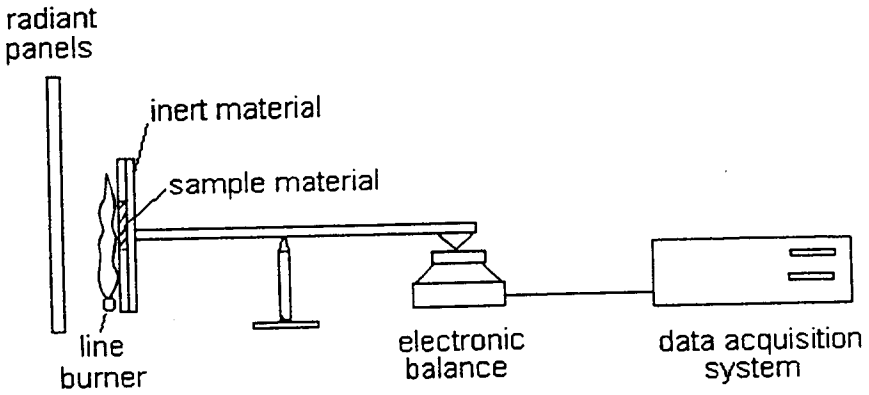

Figure C1: Experimental Mass Loss Apparatus

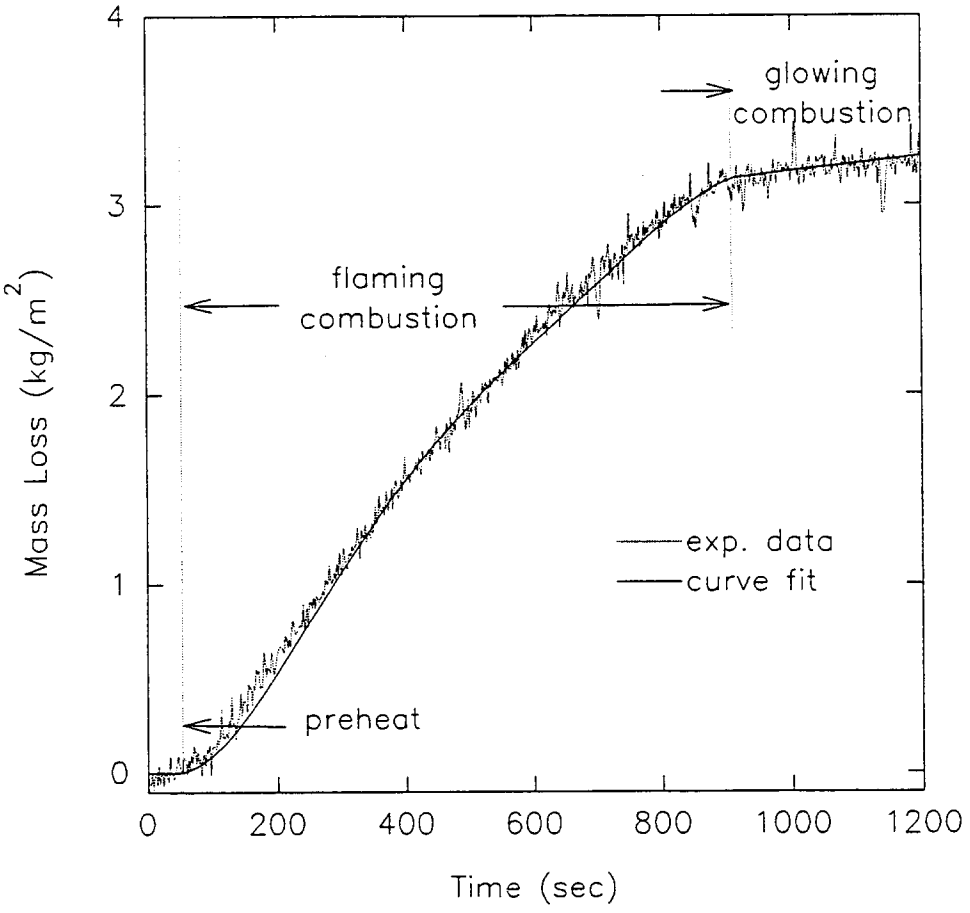

Figure C2: Mass Loss for Cardboard (with no external radiation) showing different regions of burning

rate. Obtaining mass loss rates requires that the derivative with respect to time of the original data be taken. In order to do this, a modified fifth order polynomial was used to fit the mass loss data (only in the flaming combustion region). The modification made was the removal of the first order term to result in a derivative of the curve which would yield a zero mass loss rate at t = 0. The derivative of the polynomial could easily be taken to obtain the mass loss rates, and then the peak mass loss rates chosen.

Results and Discussion

Graphs of mass loss versus time at four levels of external radiation for 3.2 mm hardboard and 15.9 mm particle board are shown in Fig. C3 and C4. Mass was lost at a higher rate for higher levels of external radiation, and the samples burned out sooner at higher levels of external radiation. The trends seen in this plot are similar to those seen for the other materials tested, namely, 3.2 mm PMMA, 5.6 mm cardboard.

The data chosen for characterizing the mass loss of the various samples are the time for mass loss to first occur (ignition time, t_{ign}) and the time for 25, 50, and 75 percent of the consumable mass of the sample to be lost (t_{25}, t_{50}, and t_{75} respectively). The data presented in Table 1 exhibit the general trend that decreasing amounts of time are required to consume a given percentage of a sample's mass as the level of external radiation is increased. Fig. C5 is a plot of half-burnout time versus radiant flux level for each material. The plot shows the expected result that half-burnout time decreases with increasing radiant flux. The half-burnout time does not decrease in proportion to the increased flux levels, and therefore, supplying higher levels of radiant flux would not be expected to proportionately enhance the mass loss rate of the samples tested.

From Table 1, PMMA showed the longest preheat times of the materials tested. PMMA, a plastic, has a well-defined ignition temperature that must be attained before pyrolysis begins. The other three materials (particle board, cardboard, and hardboard) are cellulose based materials which do not have well defined ignition temperatures. Outgassing and pyrolysis for these materials may occur over a range of temperatures.

Two other parameters commonly used to describe the flammability of a material are the peak mass loss rate and the time to peak. Table 2 lists the peak mass loss rates and time to peak as determined by the current set of tests and for previous work. The peak mass loss

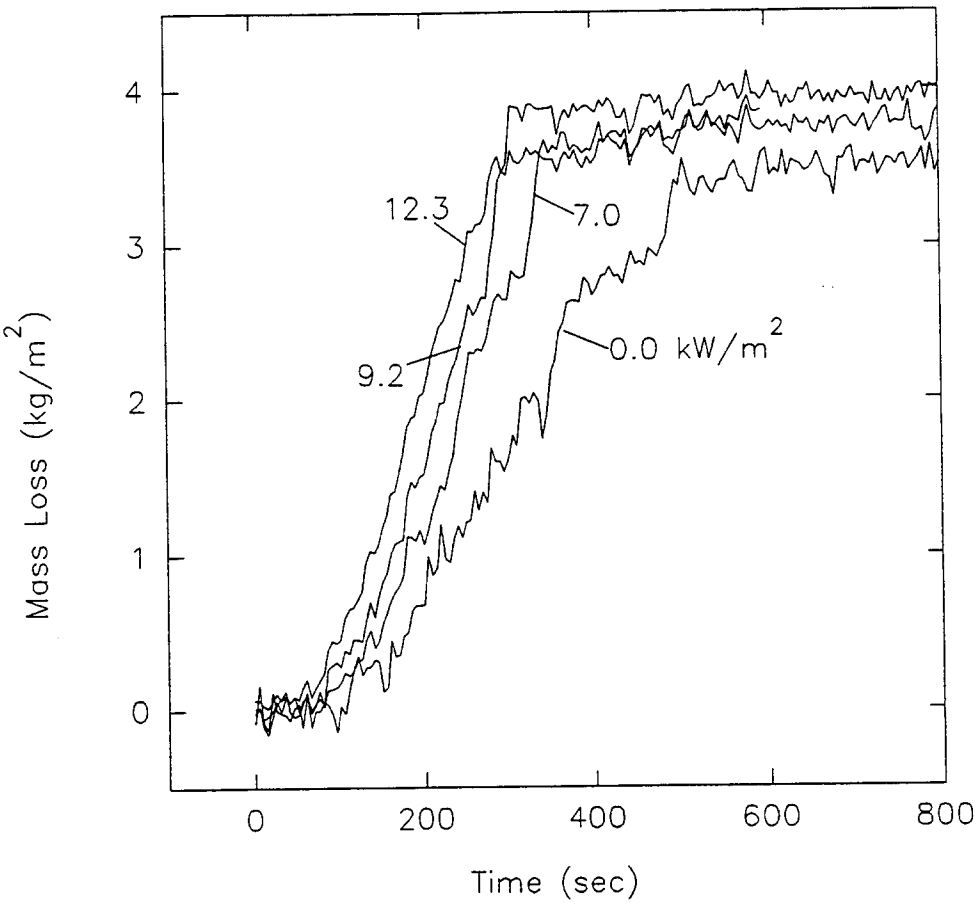

Figure C3: Mass Loss Curves for Hardboard

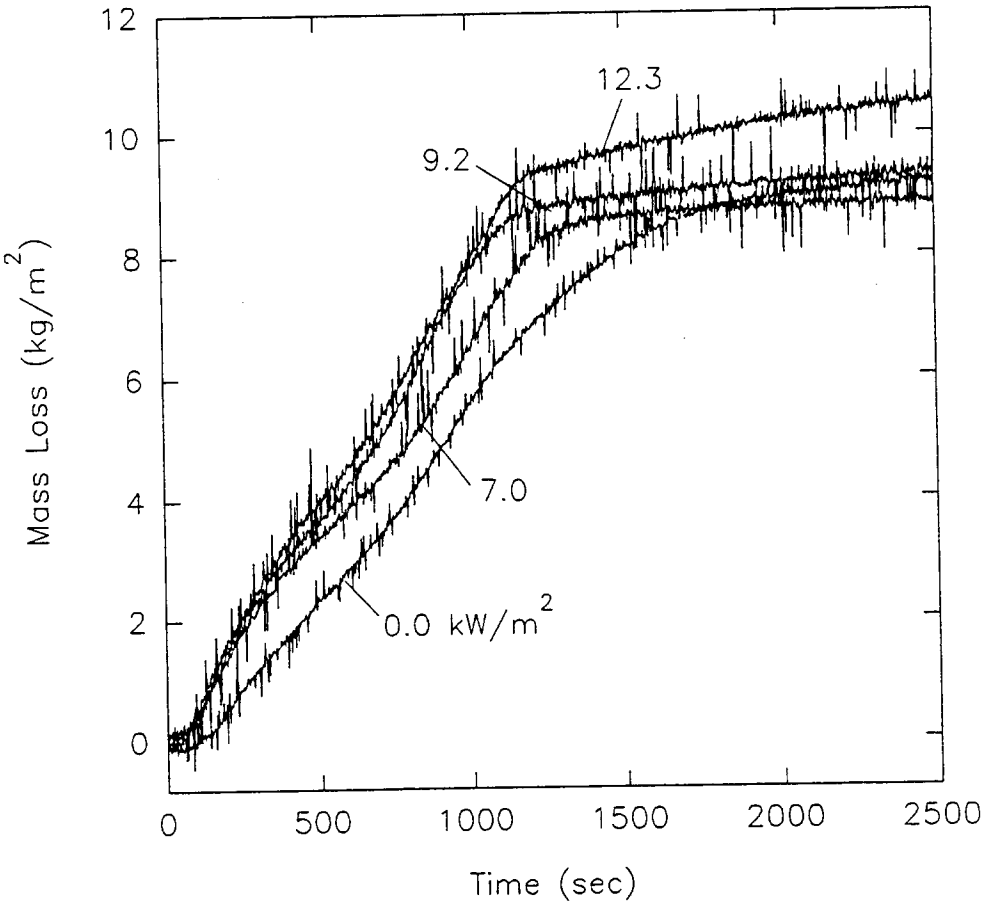

Figure C4: Mass Loss Curves for Particle Board

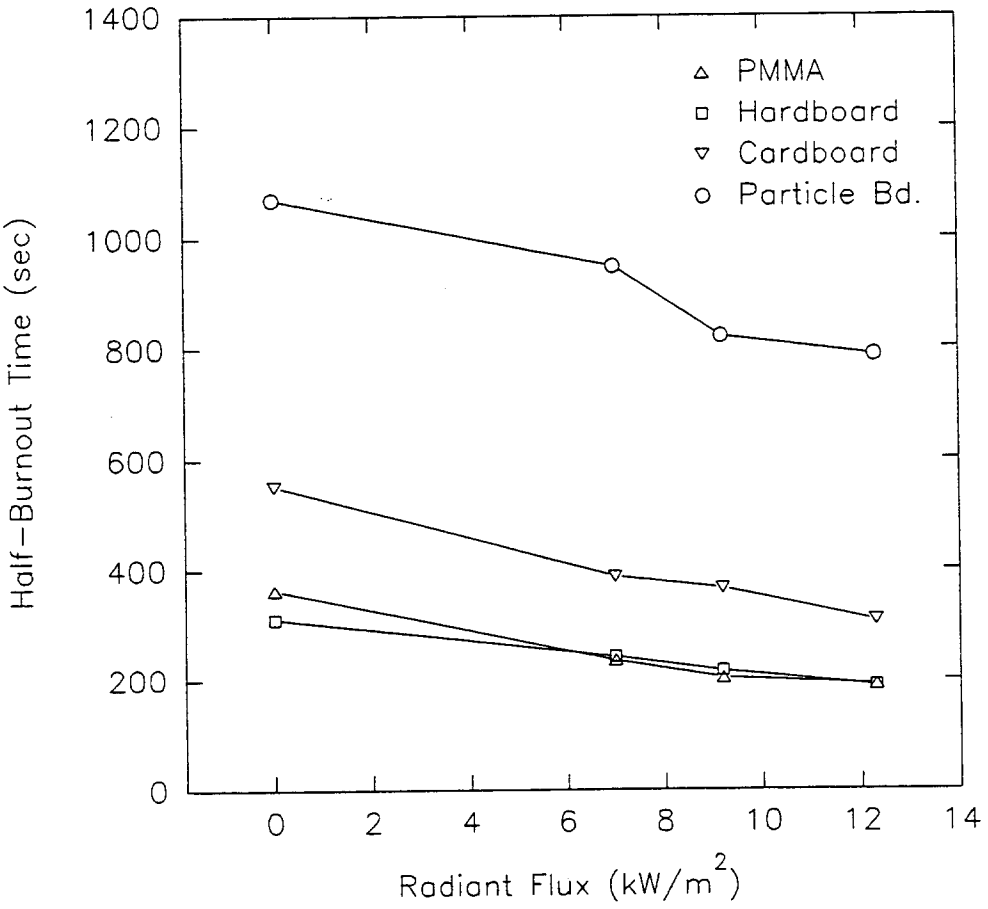

Figure C5: Half-Burnout Time as a Function of External Radiation

Material	$\dot{q}''_{er}$ (kW/m^2)	t_{ign} (s)	t_{25} (s)	t_{50} (s)	t_{75} (s)
hardboard (3.2 mm)	0.0	80	213	311	390
hardboard (3.2 mm)	7.0	35	178	239	305
hardboard (3.2 mm)	9.2	0	158	213	276
hardboard (3.2 mm)	12.3	0	130	180	238
PMMA (3.2 mm)	0.0	136	280	368	466
PMMA (3.2 mm)	7.0	90	186	243	296
PMMA (3.2 mm)	9.2	50	154	207	255
PMMA (3.2 mm)	12.3	68	149	197	240
cardboard (5.6 mm)	0.0	43	290	560	1038
cardboard (5.6 mm)	7.0	51	194	386	700
cardboard (5.6 mm)	9.2	42	184	362	636
cardboard (5.6 mm)	12.3	30	162	314	512
particle bd. (15.9 mm)	0.0	0	610	1030	2200
particle bd. (15.9 mm)	7.0	0	420	930	1430
particle bd. (15.9 mm)	9.2	0	380	806	1380
particle bd. (15.9 mm)	12.3	0	354	780	1124

Table 1. Characteristic Times associated with Mass Loss Curves

material	source	thickness (mm)	t_{peak} (sec)	$\dot{m}''_{peak}$ (kg/m^{2}s)	sample mass (g)	$\dot{q}''_{er}$ (kW/m^2)
hardboard		3.2	250	10.7×10^{-3}	53.6	0.0
hardboard		3.2	260	16.4×10^{-3}	53.6	7.0
hardboard		3.2	245	19.2×10^{-3}	53.6	9.2
hardboard		3.2	195	18.4×10^{-3}	53.6	12.3
hardboard	16#	--	--	11.1×10^{-3}	--	25.0
hardboard	16*	--	--	25.7×10^{-3}	--	20.0
hardboard	16*	--	--	24.5×10^{-3}	--	25.0
PMMA		3.2	322	10.3×10^{-3}	50.6	0.0
PMMA		3.2	216	16.7×10^{-3}	50.6	7.0
PMMA		3.2	190	16.4×10^{-3}	50.6	9.2
PMMA		3.2	170	19.8×10^{-3}	50.6	12.3
PMMA	1	25.0	--	14.6×10^{-3}	--	35.0
PMMA	1	25.0	810	41.4×10^{-3}	--	75.0
cardboard		5.6	240	5.4×10^{-3}	61.7	0.0
cardboard		5.6	166	8.5×10^{-3}	61.7	7.0
cardboard		5.6	146	8.9×10^{-3}	61	9.2
cardboard		5.6	148	9.9×10^{-3}	61.	12.3
particle bd.		15.9	622	6.8×10^{-3}	171.5	0.0
particle bd.		15.9	230	9.1×10^{-3}	171.5	7.0
particle bd.		15.9	208	9.9×10^{-3}	171.5	9.2
particle bd.		15.9	230	10.5×10^{-3}	171.5	12.3
particle bd.	4	--	--	9.9×10^{-3}	--	20.0
particle bd.	14	12.7	50	15.8×10^{-3}	--	50.0
particle bd.	15#	13.0	120	14.2×10^{-3}	--	35.0
particle bd.	15^	13.0	120	16.7×10^{-3}	--	35.0
particle bd.	17	--	--	13.5×10^{-3}	5100	25.0

1 Babrauskas
4 Smith
14 Parker
15 Tran
16 Hirschler
17 Shaw
*data obtained using the Cone Calorimeter, O_2 consumption method
#data obtained using the thermopile method, OSU apparatus
^data obtained using the O_2 consumption method, OSU apparatus
All mass loss rates reported from previous research were obtained from rate of heat release data by using a constant heat of combustion. The heat of combustion values used were: hardboard (h_c = 15000 kJ/kg), PMMA (h_c = 25600 kJ/kg), and particle board (h_c = 11600 kJ/kg).

Table 2. Peak Mass Loss Rates

rates increase with increasing levels of external radiation. Comparison with other's work shows peak mass loss rates that are on the same order of magnitude but are not directly comparable due to differences in testing (heat fluxes, sample thicknesses, and ignition methods differ). In Fig. C6, the peak mass loss rate for each material is plotted versus the radiant flux level, which demonstrates a general increase in peak mass loss rate with an increase in external radiation.

In Fig. C7, data obtained from the Cone Calorimeter and presented by Parker (1986) and Tran (1990) are compared with the current data. (Selected data points were chosen for presentation in this paper in order to give the correct shape of the curve but not the full detail of the experimental data.) Heat release rate (units of kW/m^2s) for a fuel is determined using the Cone Calorimeter by measuring the oxygen consumption of the fuel. The heat release rate (HRR) may be converted to mass loss rate by assuming a constant heat of combustion,

$$HRR = \dot{m}''(t) \times h_c. \qquad (2)$$

For particle board a value of h_c = 12000 kJ/kg was used. The Cone Calorimeter data was taken with a radiant flux level of 50 kW/m^2. Therefore, the resulting mass loss rate curve is much steeper and burnout occurs much earlier than the current data which was taken at a maximum of 12.3 kW/m^2. Also, the data from the Cone Calorimeter was measured for 12.7 mm thick particle board, and the current data was taken for 15.9 mm thick particle board. As the area under each mass loss rate curve corresponds to the mass per unit area of the sample, the area under the Cone Calorimeter curve is less. Although all samples were particle board, variations in materials making up the samples and moisture content of the samples may also contribute to differences in the data; but all methods for obtaining mass loss rate curves with external radiation resulted in the two-peak shape. The two-peak shape was also observed by Vovelle et al. (in addition to Parker (1986) and Tran (1990). The two materials that were tested and exhibited the two-peak shape were particle board and cardboard. Both are charring materials, and the second peak may be the result of a char layer forming which alters the heat transfer to the deeper material and/or the result of outgassing of volatile materials decreasing while another material has reached its pyrolysis temperature. Hardboard is also a cellulose based material, but did not show the two peak behavior. Since the hardboard sample was thinner than the other two cellulose based materials, perhaps an inhibiting char layer was not able to form, and the whole thickness of the material was pyrolyzed quickly.

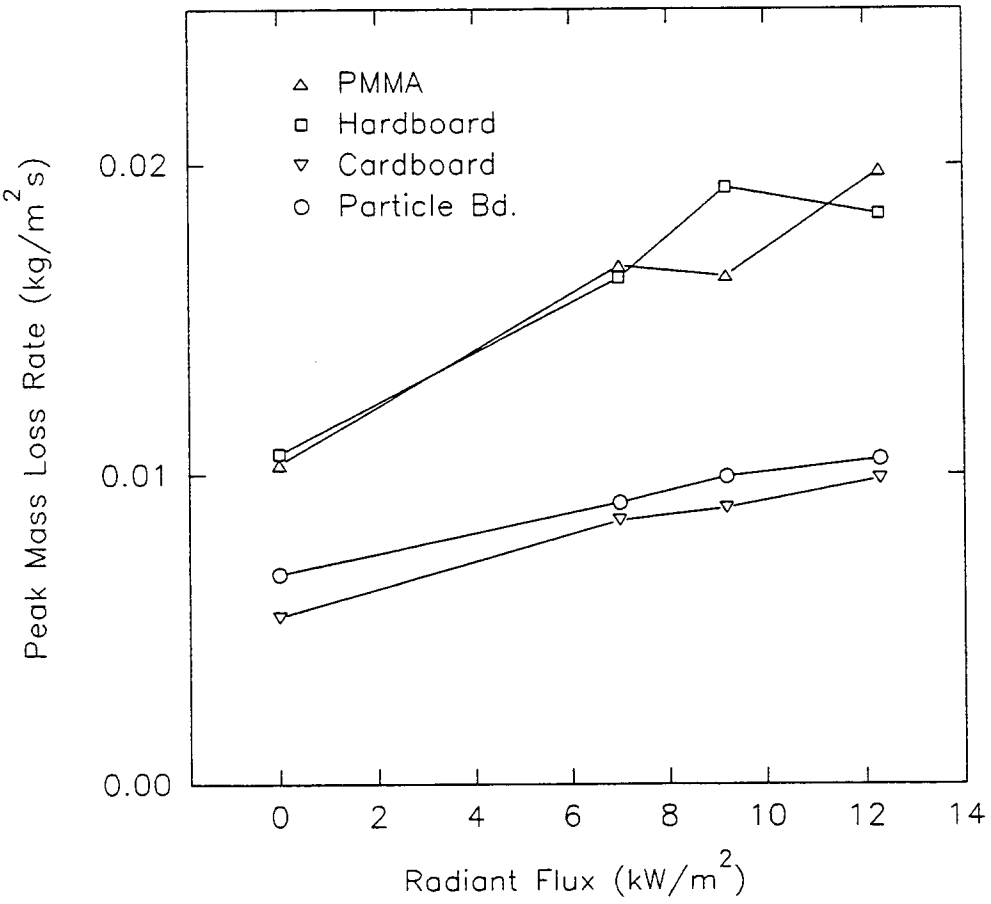

Figure C6: Peak Mass Loss Rate as a Function of External Radiation

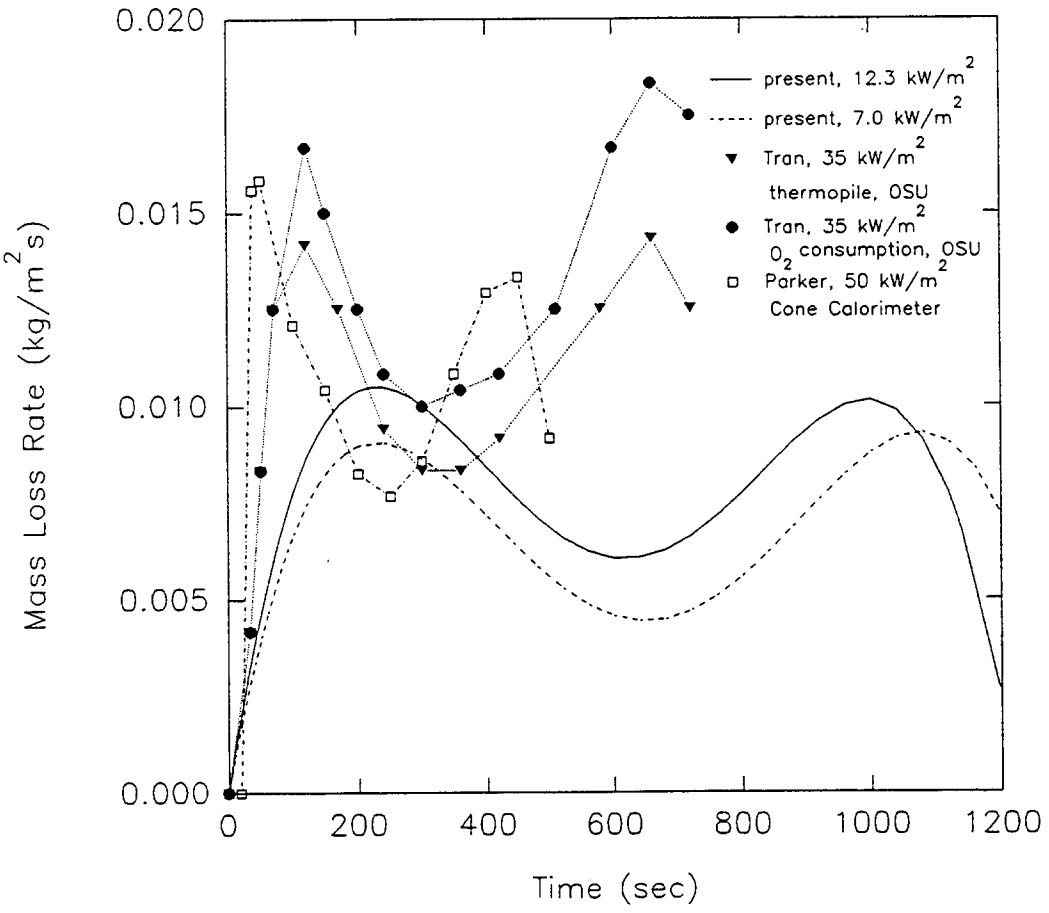

Figure C7. Mass Loss Rate for Particle Board Measured in Various Experimental Apparatuses

An alternate method to present heat release data was presented by Smith and Green (1987). They correlated the HRR with the total heat release of sample, which was a useful form for their numerical model. By properly manipulating the current data, a comparison with their data is presented in figure C8. Information on the sample thickness was not available which may account for the different scales of total heat release in the current data and the Smith and Green data. Many flame models require the input of HRR or mass loss rate histories, and therefore, the focus of this work is the presentation of data as a function of time.

Summary and Conclusions

Experimental measurements of transient mass loss r: :ardboard, PMMA, cardboard, and particle board at various levels of radiation up to 12.3 kW/m^2 were made in a configuration most similar to an upward flame spread configuration. These data can be expressed in an analytical form useful for numerical models.

As expected, the mass loss rate increases with increasing external radiation. Also, the half-burnout time decreases with increasing external radiation. For cardboard and particle board, the two-peak mass loss rate curve was observed, which is similar to the results previous investigators have obtained.

References

Babrauskas, V., 1990, *ASTM Standardization News*, January, p. 32.

Babrauskas, V., 1991, *Proceedings of the International EUREFIC Seminar 1991*, p. 89, Interscience Communications, London.

Brehob, E. G. and A. K. Kulkarni, 1993, Time Dependent Mass Loss Rate Behavior of Wall Materials Under External Radiation, *Fire and Materials*,, (to be published).

Cleary, T. G., and J. G. Quintiere, 1991, *Fire Safety Science - Proceedings of the Third International Symposium*, p. 647. Hemisphere, New York.

Fernandez-Pello, A. C., 1977, *Combustion Science and Technology*, **17**, 87.

Karlsson , B., and S. E. Magnusson, 1991, *Fire Safety Science - Proceedings of the Third International Symposium*, p. 667. Hemisphere, New York.

Kulkarni, A. K., C. I. Kim, and H. E. Mitler, 1991, Time Dependent Local Mass Loss Rate of Finite Thickness Burning Walls, *ASME Winter Annual Meeting*, Atlanta, GA.

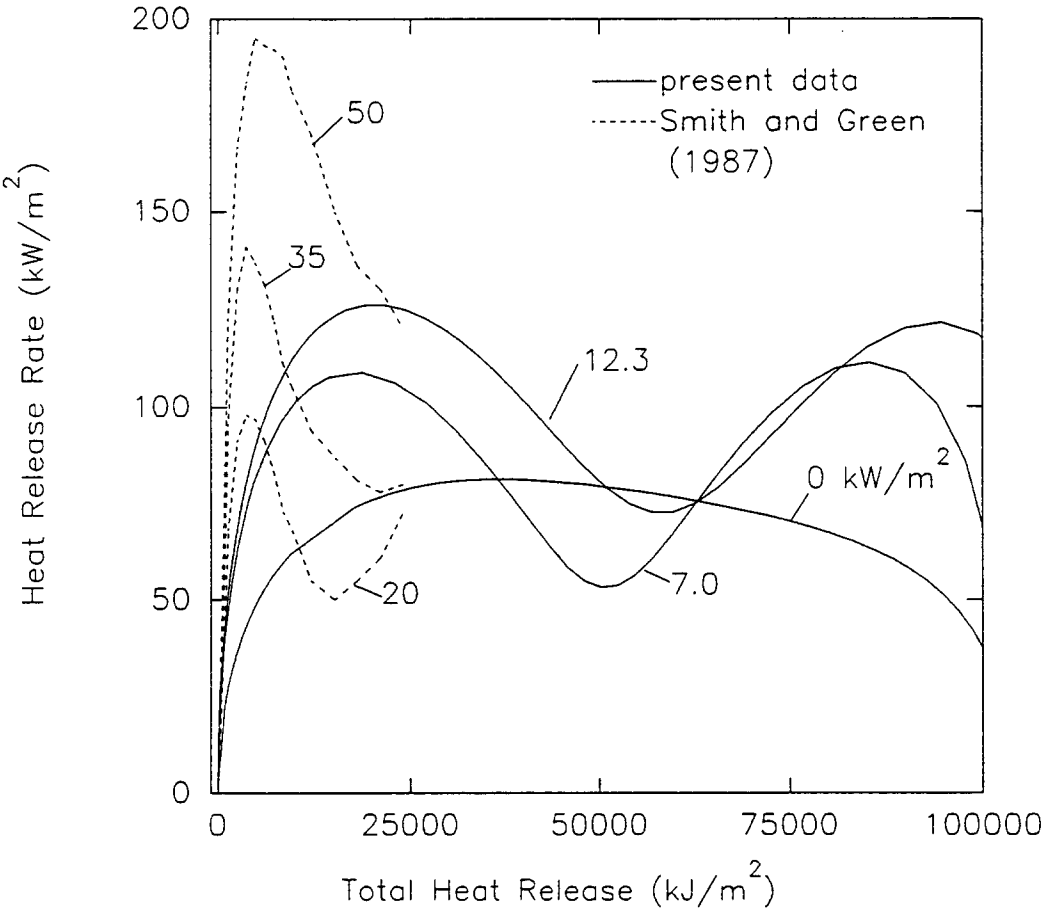

Figure 8. Heat Release Rate plotted against Total Heat Release for Particle Board

Mitler, H., 1990, *Twenty-Third Symposium (International) on Combustion*, p. 1715. The Combustion Institute, Pittsburgh.

Parker, W. J., 1986, *Fire Safety Science - Proceedings of the First International Symposium*, p. 207. Hemisphere, Washington, D.C.

Saito, K., J. G. Quintiere, and F. A. Williams, 1986, *Fire Safety Science - Proceedings of the First International Symposium*, p. 75. Hemisphere, Washington, D.C.

Smith, E. E. and T. J. Green, 1987, *Mathematical Modeling of Fires*, pp. 7-20. American Society for Testing and Materials, Philadelphia.

Vovelle, C., R. Akrich, and J. L. Delfau, 1984, *Combustion Science and Technology*, **36**, 1.

Tewarson, A., and R. F. Pion, 1976, *Combustion and Flame*, **26**, 85.

Tran, H. C., 1990, AIAA/ASME Thermophysics and Heat Transfer Conference, June 18-20, HTD-Vol. 141, Seattle, WA.

D. IN-DEPTH ABSORPTION OF EXTERNALLY INCIDENT RADIATION

(In addition to S. S. Manohar and A. K. Kulkarni, Professor S. T. Thynell was involved in this project. Dr. Thynell appreciates the support received from the Office of Naval Research under contract N00014-91-J-4116 with Dr. G. D. Roy serving as the contract monitor.)

Introduction

During flame spread along a surface, the thermal radiation emitted by high-temperature combustion products supports the advancement of the flame front. To model the response of the solid to the externally incident radiation, it is necessary to consider the spectral variation of radiative properties of the solid. For highly absorbent solids, such as wood or particle board, almost all of the externally incident radiation is absorbed at or very near the surface. However, for highly semitransparent materials, such as a plastic material whose surface is not clean, the externally incident radiation is absorbed both at the surface and within the material.

In the previous year we reported transmittance data, average transmission coefficient and Plank mean absorption coefficient for PMMA slabs. In this report, formulation and results of a transient, one-dimensional model are presented and compared with data. The spectral radiative properties employed in the radiation model were obtained from separate experiments on polymethylmethacrylate (PMMA), a clear plastic. The model demonstrates the importance of in-depth absorption. Model results exhibit the same trend as those revealed in experiments for the rise in surface temperature of the sample. Also, background, literature survey, and a description of apparatus are presented for completeness.

Nomenclature

a	absorption coefficient [m^{-1}]
C	specific heat [J kg^{-1} K^{-1}]
E	emissive power [W m^{-2}]
h	heat transfer coefficient [W m^{-2} K^{-1}]
I	radiation intensity [W sr^{-1}cm m^{-2}]
k	thermal conductivity [W m^{-1} K^{-1}]
L	thickness of slab [m]

q heat flux [W m^{-2}]
T temperature [K]; also, total transmittance
t time [s]
x distance [m]

Greek Symbols
α absorptivity
μ cos q (see Fig. D1)
λ wavelength [mm]
θ angle of directional radiation
ν wavenumber [cm^{-1}]
ρ density [kg m^{-3}]; also, reflectivity
τ transmittance of medium

Subscripts
b blackbody
e external
i initial
p at constant pressure
∞ ambient
λ,ν spectral
ν wavenumber (cm^{-1})

Superscripts
- backward
+ forward

Background

The rate of flame spread along a surface depends upon the rate at which the surface just ahead of the pyrolysis front reaches its pyrolysis temperature. The effects from both thermal radiation and convection cause rapid heating of the unpyrolyzed surface to the pyrolysis temperature. If the flame contains a high concentration of soot and if the flame temperature is 1500 K or higher, the effects of thermal radiation are of particular importance. Examples of such situations include, among others, the case of burning walls within confined

spaces where surrounding flames constitute a strong source of external radiation (Kulkarni, 1990; Ito et al., 1992) and emission from plumes of burning liquid pools (Klassen et al., 1992). To model the thermal response of semitransparent materials exposed to externally incident radiation, it is necessary to consider the effects of in-depth absorption, which includes spectral variation of the radiative properties.

Park and Tien (1990) performed a detailed analysis of the heating up and ignition of solid fuels subjected to radiation which included volumetric radiation absorption in both the gaseous and solid phases. For in-depth absorption in the solid, they used a gray model with a constant value of 100 cm^{-1} for the absorption coefficient. A nongray radiation model was employed by Song and Viskanta (1990) to study heating of ice by external radiation using a multiband, spectrally-dependent absorption coefficient. Using a gray model, Finlayson et al. (1987) studied temperature profiles caused by in-depth absorption in polymeric solids and compared them to the opaque case. For clear plastics, such as polymethylmethacrylate (PMMA), the absorption coefficient is highly wavenumber-dependent and much smaller (i.e., the radiation is absorbed much deeper inside the solid). As a result, it is necessary to accurately measure the spectral variation of the absorption coefficient in order to adequately model the volumetric absorption of the incident radiation.

Flame spread driven by externally incident radiation has been studied experimentally and theoretically (Saito et al., 1989, and Fernandez-Pello, 1977). However, these models treated the medium as opaque. Such an assumption results in a more rapid rise in surface temperature and consequently in a greater rate of predicted flame spread. On the other hand, in-depth absorption results in distribution of the incident radiant energy within the material, and hence the surface temperature rises at a lower rate.

In order to improve the predictive capabilities of ignition and flame spread across semitransparent materials, it is important to account for a spectral variation of the in-depth radiation absorption in the model. In particular, prediction of surface temperature requires detailed treatment of the interfacial conditions between the gas and solid phases. PMMA is a material commonly used in many practical applications as well as in flammability testing. The objective of the present work is to study the effects of in-depth radiation absorption on the surface temperature of a semitransparent material, using PMMA as an example. Analysis for a problem of one-dimensional, transient, conduction with volumetric spectral radiation absorption is carried out and solved numerically to determine the surface temperature. The model accounts for spectral variation of the absorption coefficient and reflectivity. These

properties are determined for PMMA using a Fourier transform infrared (FTIR) spectrometer. Experiments are conducted to measure the surface temperature of PMMA slabs subjected to a range of flux levels of externally incident radiation. The effect of in-depth absorption is then evaluated by comparing surface temperature histories of semitransparent slabs with clear versus absorbing front surfaces obtained from both model and experiments.

Mathematical Model

Assumptions

A schematic of the model is shown in Fig. D1. The medium considered is either semi-transparent or opaque. In a real fire situation, the surface well above the pyrolysis front may be clear initially, but becomes covered with a layer of soot as combustion progresses. Hence, it is necessary to consider one situation when the surface is clear and the other when the surface is covered with a layer of soot or dust. When the surface is covered with a layer of soot, most of the external radiation is absorbed at the surface, but the soot layer may reradiate some of this energy into the semitransparent medium and into the surroundings. However, if the medium is opaque, reradiation takes place in the surroundings only. When the surface is free of soot or dust, in-depth radiation takes place in the case of a semitransparent medium, whereas the opaque medium either reflects or absorbs the incident radiant energy at the surface. Based on the above description, the mathematical model considers the following four cases:

Case 1: The front surface is clear, and the medium is semitransparent.

Case 2: The front surface is clear, and the medium is opaque.

Case 3: The front surface is absorbing (soot-covered), and the medium is semitransparent.

Case 4: The front surface is absorbing (soot-covered), and the medium is opaque.

The difference in the thermal response between case 1 and case 2 illustrates the effect of in-depth absorption for clear samples, and the difference in the thermal response between case 3 and case 4 reveals a similar effect for surface-absorbing samples. The purpose of the proposed model is to predict the thermal response of the semitransparent or opaque medium. It employs the following set of assumptions:

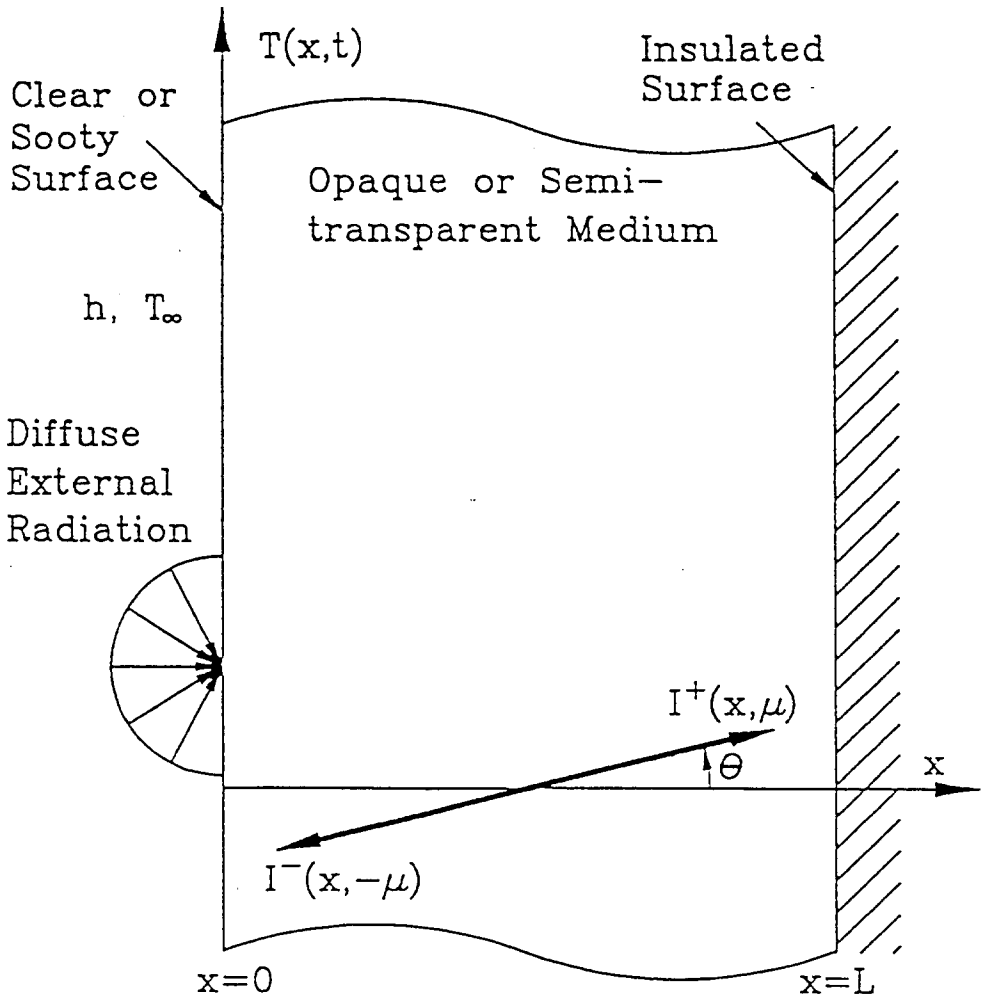

Figure D1: Schematic of mathematical model

(1) The temperature distribution within the medium is one-dimensional and transient.

(2) The front surface at $x = 0$ is subjected to externally incident radiation and convection.

(3) The back surface at $x = L$ is insulated and neither receives nor reflects any thermal radiation.

(4) The externally incident radiation is diffuse.

(5) Emission of thermal radiation from and scattering within the semitransparent medium is neglected.

(6) The soot layer is a perfect emitter and a perfect absorber of thermal radiation.

(7) The normal spectral reflectivity obtained from measurements of PMMA is approximately equal to the hemispherical spectral reflectivity.

(8) The spectral emissive power of the external source is based on calibration measurements at the sample location, gray emissivity of the panel's surface, and temperature measurements of the heated panels.

(9) Properties of PMMA are independent of temperature in the range of interest. (Tewarson and Ogden, 1992)

(10) Properties of surrounding air are temperature dependent.

Some of the above assumptions require further explanation. Regarding assumption 1, the length and width of a slab or wall material is usually much greater than its thickness in most applications of interest; therefore, the parameters of interest do not vary significantly with length or width. Assumption 3 is based on the fact that thermal wave penetration is not deep for the thick samples (typically 19 mm) employed in our relatively short experiments, and that in-depth radiation absorption in PMMA is significant only up to a depth of about 4 mm for the wavenumbers of interest (Daikoku et al., 1991). For further justification of assumptions and more details, please refer to Manohar (1992).

Formulation

The energy equation within the solid is given by

$$k\frac{\partial^2 T}{\partial x^2} - S(x) = \rho C_p \frac{\partial T}{\partial t}, \quad 0 < x < L, t > 0,$$

with initial condition

$$T = T_i, \ 0 \le x \le L, \ t = 0$$

and boundary condition

$$\frac{\partial T}{\partial x} = 0, \ x = L, t > 0.$$

The boundary conditions at $x = 0$, $t > 0$, are as follows:

Case 1: Semitransparent solid with clear surface

$$h(T_\infty - T) = -k\frac{\partial T}{\partial x}$$

Case 2: Opaque solid with clear surface

$$\int_0^\infty (1-\rho_{e,\nu}) q_{e,\nu} d\nu + h(T_\infty - T) = -k\frac{\partial T}{\partial x}$$

Because the surface reradiation term is expected to be small for samples with clear surfaces, it is not included in the above energy balance. This also ensures that the same amount of energy is deposited on the opaque and semitransparent solids; consequently, the differences in surface temperature between cases 1 and 2 are due to in-depth absorption.

Case 3: Semitransparent solid with surface covered with soot

$$q_e + h(T_\infty - T) - 2E_b[T(0,t)] = -k\frac{\partial T}{\partial x}$$

Case 4: Opaque solid with surface covered with soot:

$$q_e + h(T_\infty - T) - E_b[T(0,t)] = -k\frac{\partial T}{\partial x}$$

The source term in equation (1) is

$$S(x) = -\frac{\partial q_r}{\partial x},$$

and for the opaque medium, it is

$$S(x) = 0 .$$

In order to estimate the convective heat transfer, it is necessary to determine the heat transfer coefficient. The Nusselt number is determined using a correlation for a vertical surface at constant temperature since variation of temperature along the surface is not significant (Churchill and Chu, 1975). During the experiments, however, the surface temperature is expected to vary from about 298 to 570 K; therefore, variable properties of air are used. For a semitransparent medium, S(x) is obtained by considering energy transfer by radiation. The equation of transfer for a nonscattering and nonemitting medium is given by (Manohar, 1992),

$$\mu\frac{\partial I_\nu(x,\mu)}{\partial x} + a_\nu I_\nu(x,\mu) = 0 , \quad 0 < x < L, \ -1 \le \mu \le 1$$

The radiation intensity is split into a forward I^+ and backward direction I^-. The boundary conditions at x = 0 and x = L, corresponding to the two cases involving a semitransparent medium described above are, respectively, given by

Case 1 : $I_\nu^+(0) = (1-\rho_\nu)\, q_{e,\nu} / \pi$

Case 2 : $I_\nu^+(0) = E_{b,\nu}[T(0,t),\nu] / \pi$

$$I_\nu^-(L,-\mu) = 0, \quad \mu > 0$$

The solution to the radiation problem is immediately found as

$$I_\nu^+(x,\mu) = I_\nu^+(0)\exp(-a_\nu x/\mu) , \qquad \mu > 0,$$

$$I_\nu^-(x,-\mu) = 0, \qquad \mu > 0.$$

Integration over all solid angles and wavenumbers yields an expression for the source term of the form

$$S(x) = 2\pi \int_0^\infty a_\nu I_\nu^+(0)\, E_2(a_\nu x) d\nu$$

where $E_2(x)$ is the exponential integral function. Spectral absorption coefficient and reflectivity are determined experimentally, as discussed in the following section. Finally, a solution to the transient heat conduction problem is obtained using the Crank-Nicholson scheme. The resulting finite-difference equations were solved using a Digital VAX computer.

Experiments

Two series of experiments were conducted: radiation property measurements for input to the model; and transient surface temperature measurements for a slab in the presence of strong external radiation to verify the model.

Absorption Coefficient and Reflectivity

The mathematical model requires input of the spectral absorption coefficient and reflectivity of the surface. These properties were deduced from measurements, using an FTIR spectrometer. A wavenumber range from 12,000 to 500 cm^{-1} was covered through two different combinations of detector and beam splitter. A potassium bromide beam-splitter was used with a mercury-cadmium- telluride (MCT) detector, and a lead selenide detector was used with a quartz beam splitter. Details of the FTIR experiments can be found in Manohar (1992). The data reduction procedure discussed below is similar to that used by Myers et al. (1983).

The spectral data obtained using the spectrometer represent the total transmittance ($\mathcal{T}_\nu$), that is, it accounts for multiple reflections within the semitransparent medium. To deduce the transmissivity (τ_ν) and reflectivity (ρ_ν), one employs the relationship (Siegel and Howell, 1981),

$$\tau_v = \frac{-(1-\rho_v)^2+\sqrt{(1-\rho_v)^4+4\,T_v^2\rho_v^2}}{2T_v\rho_v^2}.$$

Transmittance data (T_v) for at least two different sample thicknesses are necessary in order to solve for the two unknowns (α_v) and (ρ_v) at each wavenumber. The resulting pair of nonlinear, simultaneous equations is readily solved using the available software NEQNF (IMSL, 1984). Data for three different combinations of sample thicknesses were obtained and values were averaged. The repeatability of the transmittance data was verified by conducting additional experiments for another set of samples of the same thickness. Finally, the absorption coefficient, a_n, is calculated from

$$\tau_v = \exp(-\alpha_v L).$$

Surface Temperature Measurements

In order to verify the accuracy of the model discussed above, experiments were carried out to determine the rise of surface temperature on two sets of PMMA samples subjected to a range of heat fluxes. In the first set, clear samples were used. In the second set, samples were covered with a flat black paint to simulate the presence of a layer of soot.

Figure D2 shows the experimental setup. A 12 cm x 12 cm x 1.9 cm PMMA sample was mounted in a sample holder. The sides and back face of the sample holder were insulated with ceramic fiber and then mounted on a steel framework. The sample was then subjected to external radiation by radiant panels placed in front of it. The power supplied to the radiant panels was varied with a silicon control rectifier (SCR) controller.

Four grooves were cut into the sample, two on the front face and two on the back face. Thermocouples of 100 mm diameter were mounted in these grooves. A few drops of a volatile solution added to the grooves then dissolved a small amount of PMMA. A thin layer of PMMA formed on the thermocouple bead and its wires ensured that the temperature read by the thermocouple was essentially that of the surface of the sample. The thermocouples were connected to a digital data acquisition system.

The error in surface temperature measurements was mainly due to the size of the junction and the uncertainty in positioning the thermocouple junction at the surface (about

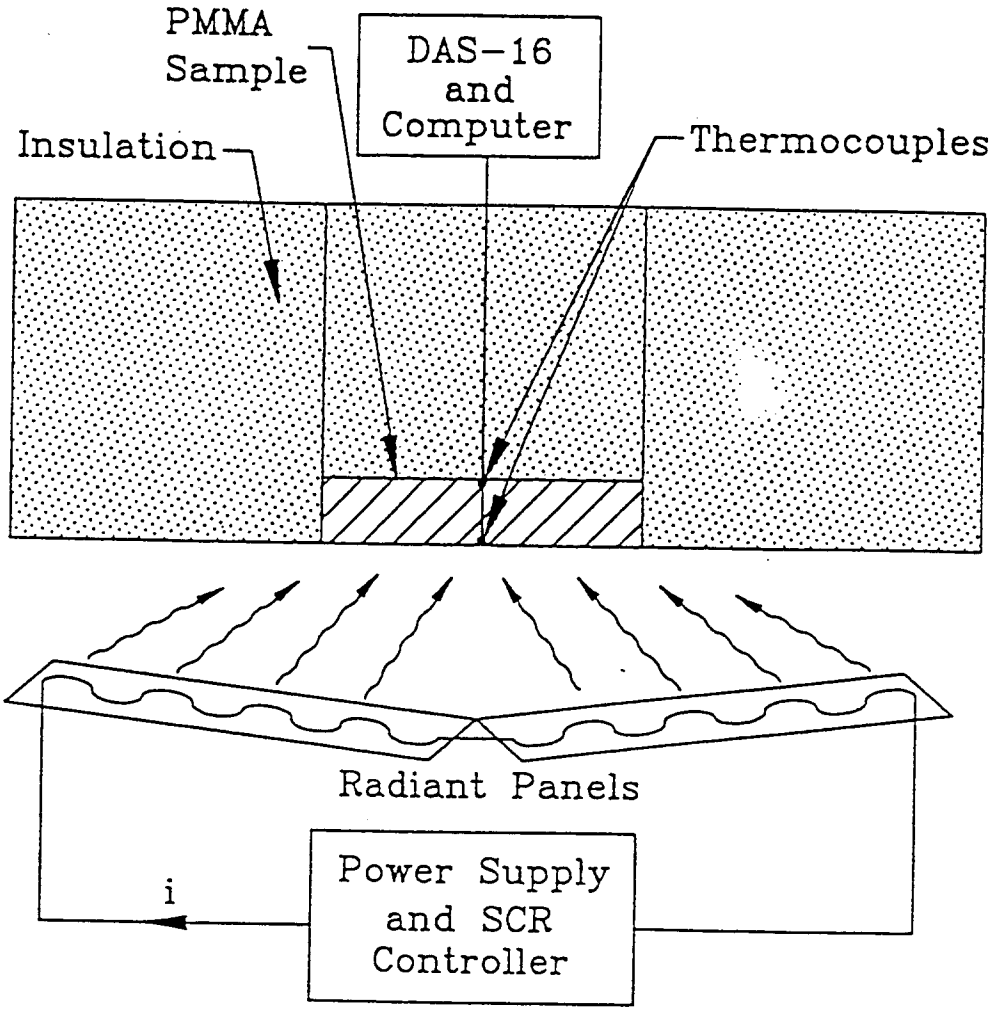

Figure D2: Schematic of experimental setup

0.5 mm), and the magnitude depended on the temperature gradient at the surface (between 6 to 40 degrees per mm for heat flux between 3.7 and 16.2 $kW/m^{2)}$. In addition, there was an error due to difference in emissivities of thermocouple junction and PMMA surface, an error in measuring the heat flux itself (about 10 to 20% depending on heat flux level), and scatter in data (about 1.5 degrees). Thus, the surface temperature data are accurate to within +/- 5 to 25 degrees. Since there are uncertainties in the model due to inexact property data and other assumptions, it is important to compare the data and model calculations *qualitatively*, while model calculations at various conditions can be compared *quantitatively*. The experiments were conducted primarily to observe any obvious relative effects of depth absorption on temperature profiles, and to observe the general trends of temperature at various conditions.

Results and Discussion

Radiation Properties

Figure D3 presents typical transmittance data obtained for clear PMMA samples 0.8 mm thick. Samples of greater thickness revealed a much lower transmittance in the near- and mid-infrared wavenumber ranges. It can be seen that transmittance is very low in the region from 1000 to 3000 cm^{-1}. This may be explained by examining the molecular structure of PMMA. The monomer unit of PMMA is $C_5H_8O_2$. The region around 1000 cm^{-1} corresponds to the bending of C-H, C-O-C and C=O groups and the twisting frequencies of the methyl (CH_3) and methylene (CH_2) groups. The region around 3000 cm^{-1} corresponds to the stretching frequency of the C-H bond in the methyl group (Silverstein et al., 1981). This region has a high reflectivity, which accounts for the low transmittance values. Transmittance was also measured for soot-covered samples, and it was found to be negligible compared to that of the clear samples due to high absorption in the soot layer on the surface.

Figures D4 and D5 show the deduced spectral absorption coefficient and reflectivity, respectively. The absorption coefficient data in the region 1000 to 3000 cm^{-1} shows a number of spikes. As can be seen from Fig. D3, the transmittance in this region is very low. Also shown in Fig. D4 is the blackbody radiation spectrum at 1000 K and the 14-band model for the absorption coefficient. It should be noted that only 25% of the incident energy from a source having an equivalent blackbody emission at 1000 K is contained in the spectrum

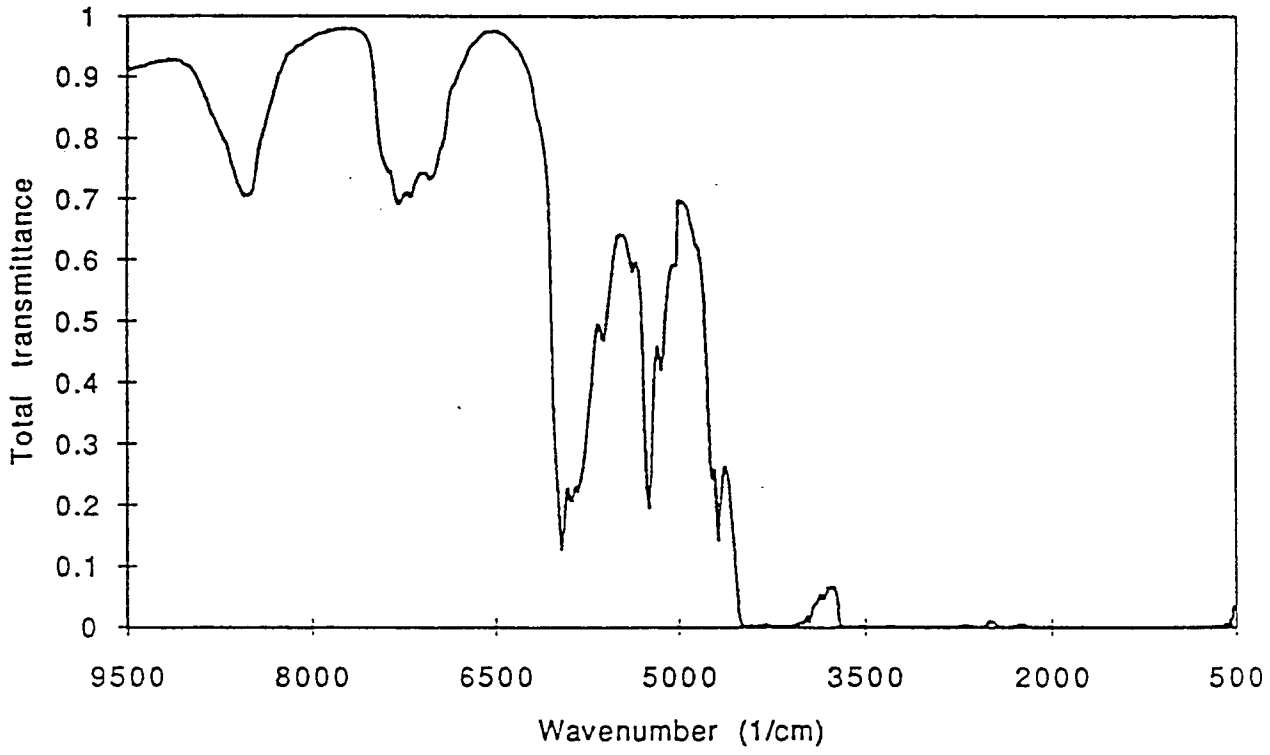

Figure D3: Typical transmittance data for a 0.8 mm thick PMMA slab

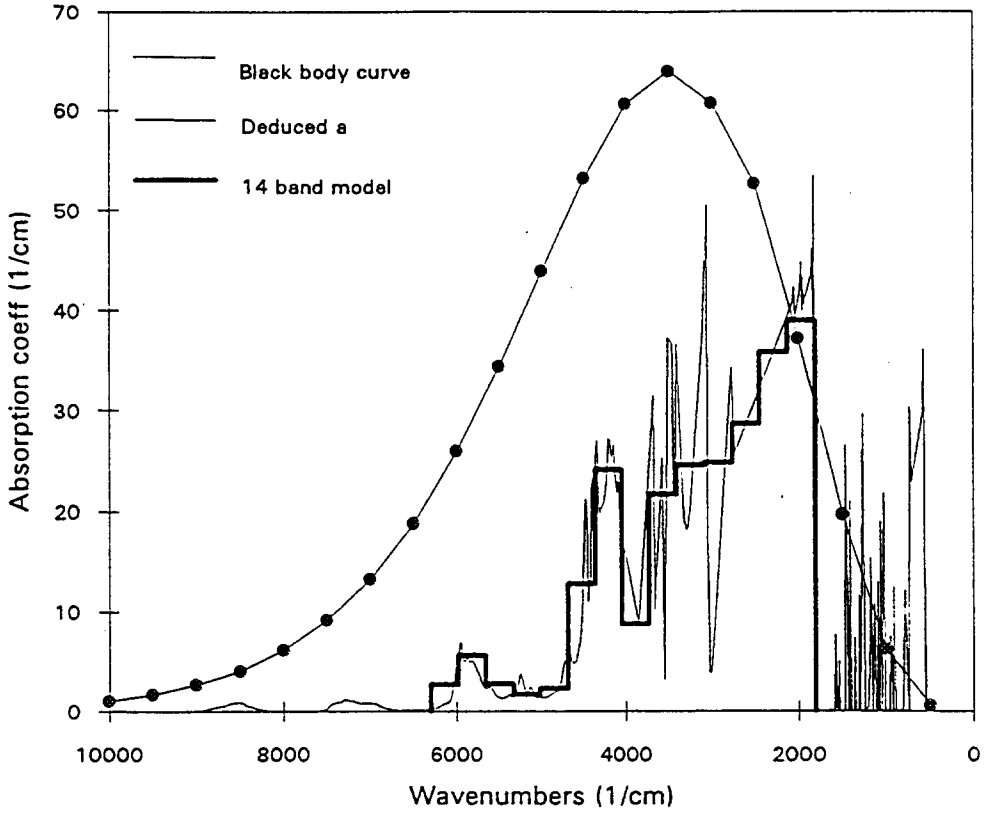

Figure D4: Spectral absorption coefficient and the 14 band model. The superimposed blackbody curve shows the distribution of energy in this wavenumber regime

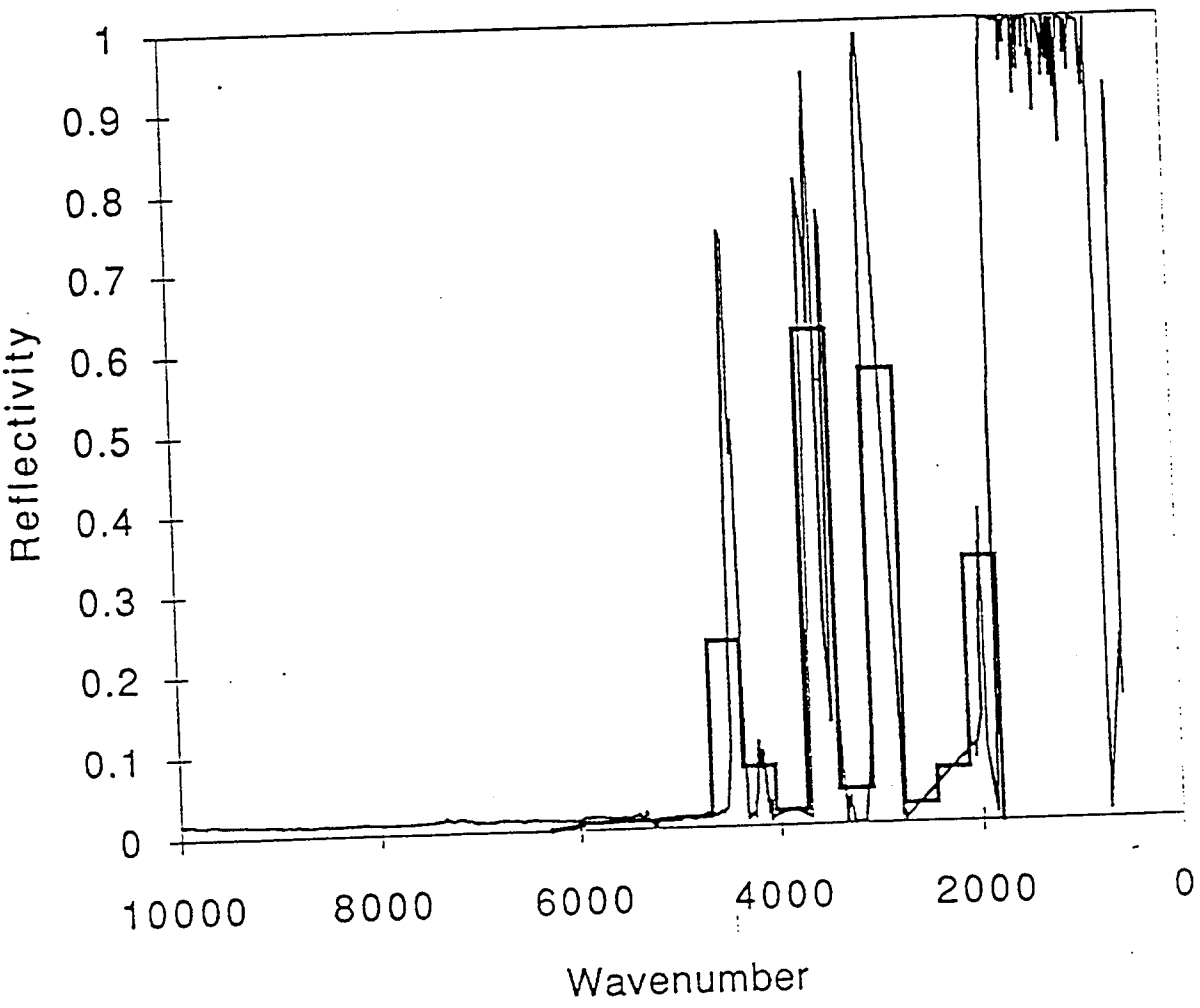

Figure D5: Spectral reflectivity and the 14 band model

above 3300 cm^{-1}. On the other hand, the spectral absorption coefficient changes in a highly nonlinear manner with the wavenumber, then rapidly diminishes above 3300 cm^{-1}. The band model range is selected in such a way that below 1775 cm^{-1} and above 6250 cm^{-1} absorption of radiant energy changes from a volumetric to a surface phenomenon because the transmittance is negligible in those regions. The range between these two values is divided into 14 equal intervals, and within each interval the absorption coefficient is uniform. It should be noted that the in-depth absorption depends on both the spectral distribution of incident radiation and the spectral properties of the absorbing medium. Therefore, a carefully selected multiband model must be used in addressing the radiation problem. Table 1 shows the details of the experimentally determined band model used in the :nt problem.

Surface Temperature Measurements

Experiments were carried out for clear and blackened samples, using five different heat fluxes ranging from 3.7 to 23.2 kW/m^2. Experimental data were recorded until either steady state was reached or the surface of the sample was completely covered with bubbles. Figures D6a and D6b show the measured surface temperature of clear and surface-blackened PMMA samples for different heat fluxes. For the lowest level of heat flux (3.7 kW/m^2), bubbles did not form at the surface of the PMMA sample as the sample tended towards steady state. With an increase in the external flux, the rate of temperature rise became far more pronounced, with bubbles forming rapidly just beneath the surface. Because of convective loss at the surface and in-depth absorption, the highest temperature in the solid occurs at an interior location, not at the surface. Therefore, formation of bubbles under the surface is an indication of in-depth absorption. Recovered samples showed bubble formation just beneath the surface. For the highest heat flux, the time required for bubble formation was an order of magnitude smaller compared to the lowest applied heat flux. For blackened PMMA samples, the general nature of the temperature rise was the same as in the clear samples. However, as the temperature of the surface increased, the time required for bubble formation at the surface decreased. This is to be expected, since a larger fraction of the externally incident radiation is absorbed by the blackened PMMA surface compared to the clear PMMA surface.

Table 1 - A 14-band model for spectral absorption coefficient and reflectivity.

Wavenumber range (cm^{-1})	Absorption coefficient (cm^{-1})	Reflectivity
1800 - 2122	38.95	0.33
2122 - 2444	35.85	0.066
2444 - 2766	28.64	0.024
2766 - 3088	24.74	0.5643
3088 - 3410	24.53	0.0431
3410 - 3732	21.65	0.6151
3732 - 4054	8.70	0.019
4054 - 4376	24.07	0.0732
4376 - 4698	12.77	0.2301
4698 - 5020	2.26	0.013
5020 - 5342	1.70	0.0099
5342 - 5664	2.74	0.0097
5664 - 5986	5.55	0.0092
5986 - 6308	2.68	0.0061

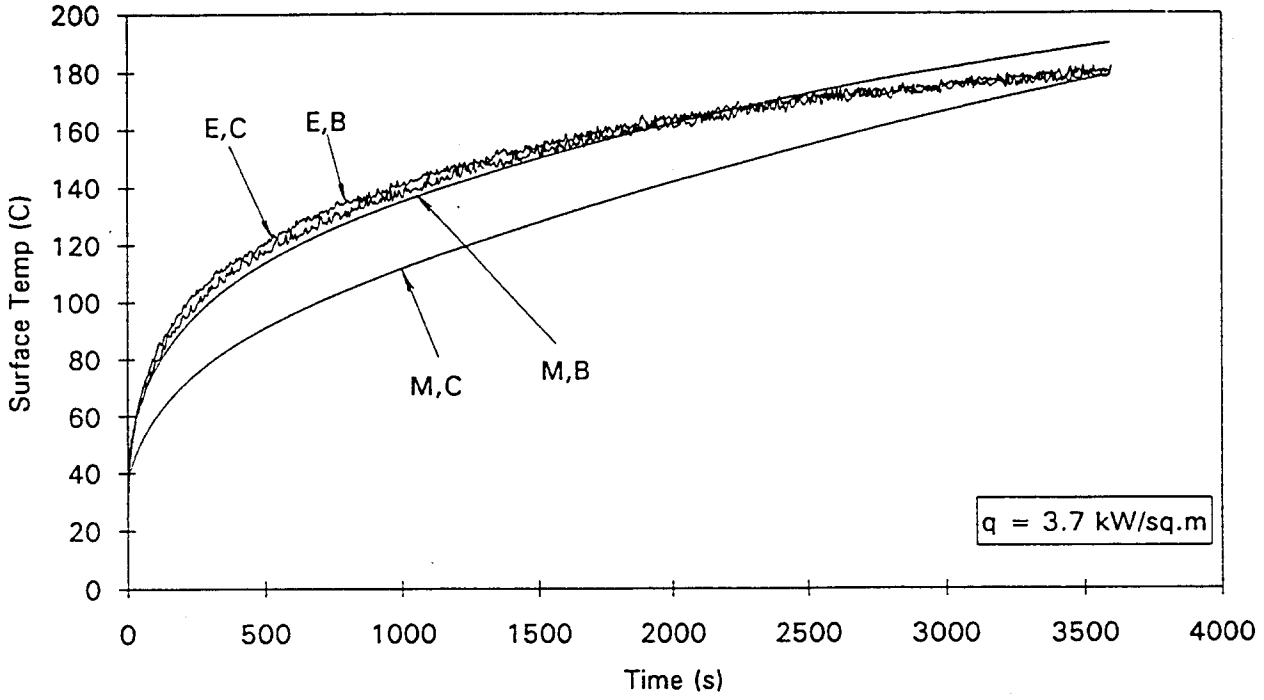

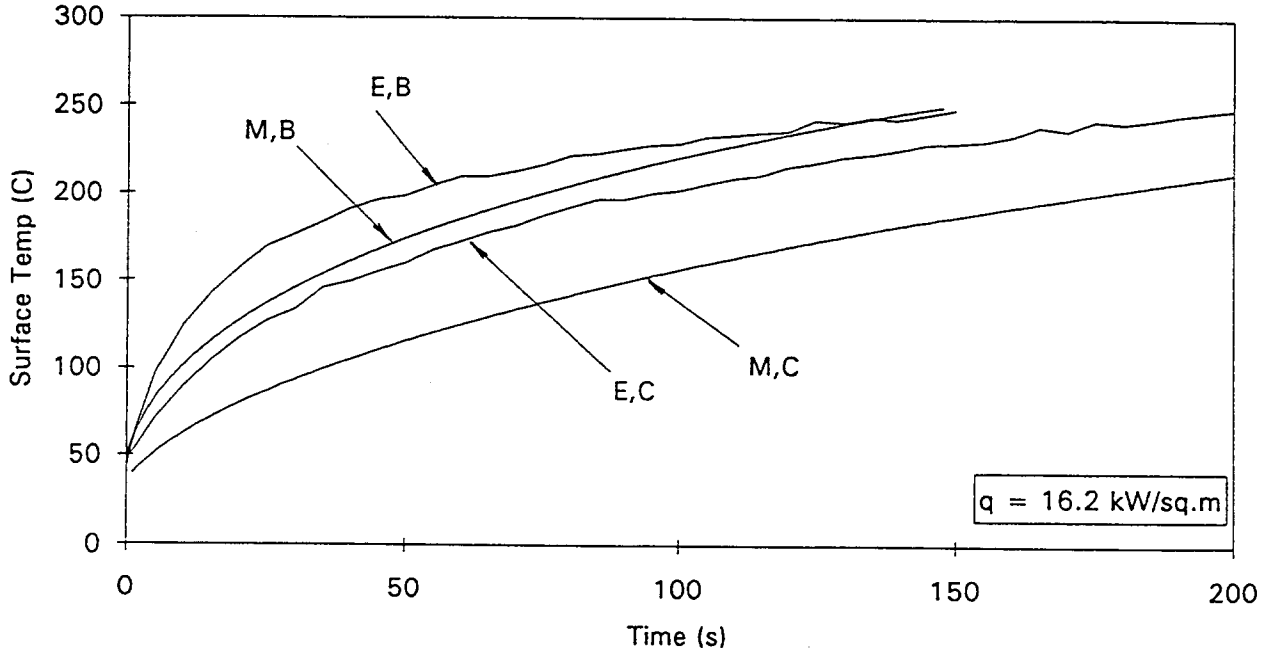

Figure D6: Comparison between surface temperatures obtained by model and by experiment for clear and blackened surfaces (a) at an external heat flux of 3.7 kW/m^2 and (b) at an external heat flux of 16.2 kW/m^2. E - Experiment, M - Model, C - Clear surface, B - Blackened surface.

Analytical Results

For a given surface condition, the difference between the opaque and semitransparent case represents the effect of in-depth radiation absorption. Figure D7 shows the temperature profiles obtained for semitransparent and opaque media for different heat fluxes. Since in-depth absorption distributes energy within the solid, the surface temperature is expected to rise at a slower rate. The temperature profiles intersect just below the surface because the total energy deposited into the solid is the same, except for the convective loss. (Since the surface temperatures are different, the convective loss from the opaque medium is greater than that of the semitransparent medium; therefore, the two curves do not meet later.)

In applications such as upward flame spread, the heat-up time (time required to reach a critical temperature) is an important parameter. Figures D8a and D8b show the effect of in-depth absorption on the rise of surface temperature at two different fluxes. As a representative case for the clear samples, the time required for the surface temperature to reach 150 C for the clear surface is recorded in Table 2 for several heat fluxes. A temperature of 150 C is selected because the bubble formation does not occur at this temperature. At low heat fluxes, the difference is on the order of 10 %. The temperature rise for both media is slow, and the surface temperature asymptotically reaches steady state. At higher heat fluxes, however, there is a significant increase in the heat-up time for the semitransparent sample, which requires more than twice the time to reach 150 C at a heat flux level of 16.2 kW/m^2 compared to the opaque sample. Clearly, a semitransparent medium will support upward flame spread at a slower pace than a similar opaque medium.

For blackened samples, it is observed that there is practically no difference in the rise of surface temperature for the two media. Both absorb the externally incident flux at the surface. Energy reradiated inwards by the semitransparent medium's blackened surface is then absorbed in depth. This fraction of energy does not noticeably affect the surface temperature. The time required for the surface to reach a critical temperature is virtually the same. For the cases considered in this work, in-depth absorption does not significantly affect the thermal response of media with blackened surfaces.

Comparison with Experiments

The model results are compared to the experiments in Figures D6a and D6b. Examination of these figures reveals a discrepancy between the model prediction and experiments. There are several reasons for this discrepancy. First, the model uses measured

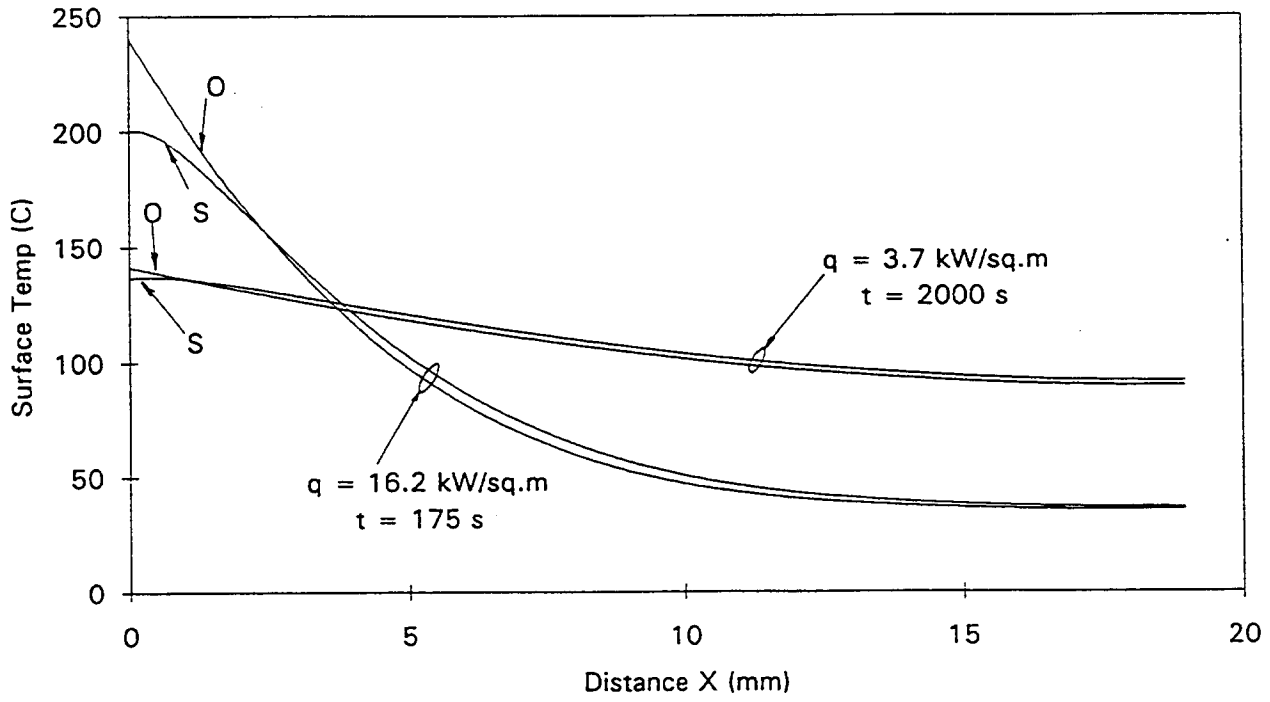

Figure D7: Theoretical temperature profiles. O - Opaque medium, S - Semitransparent medium

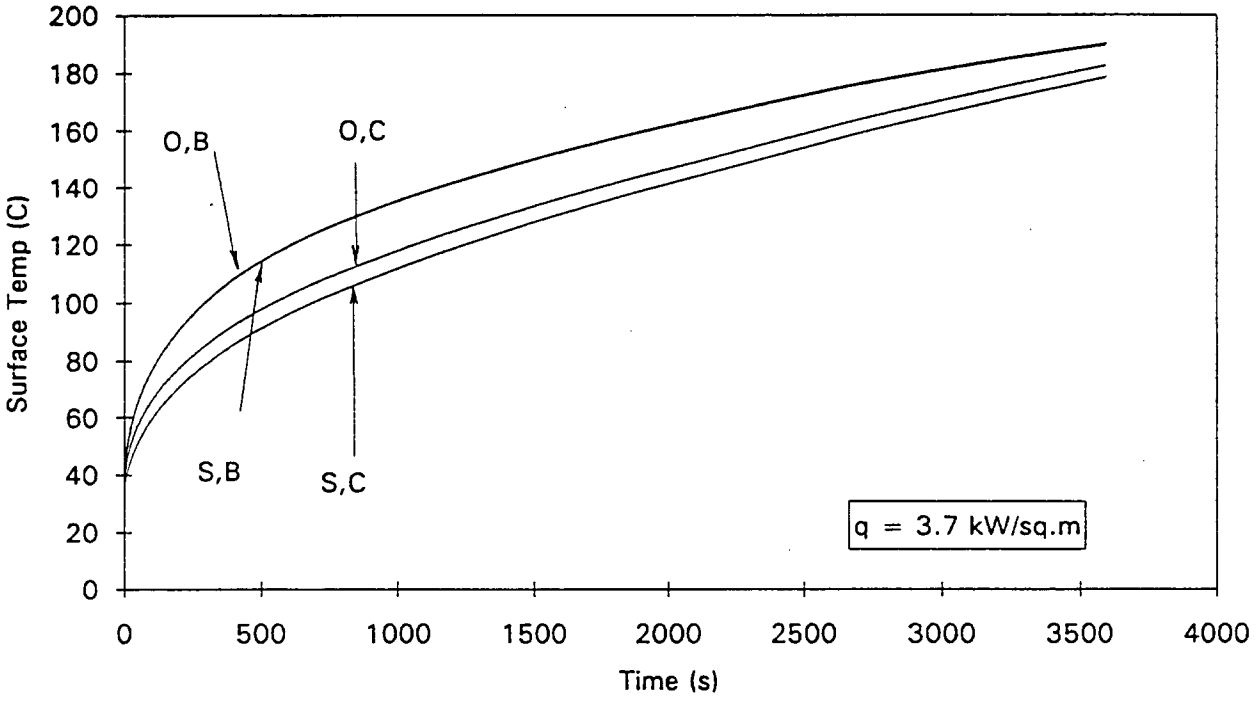

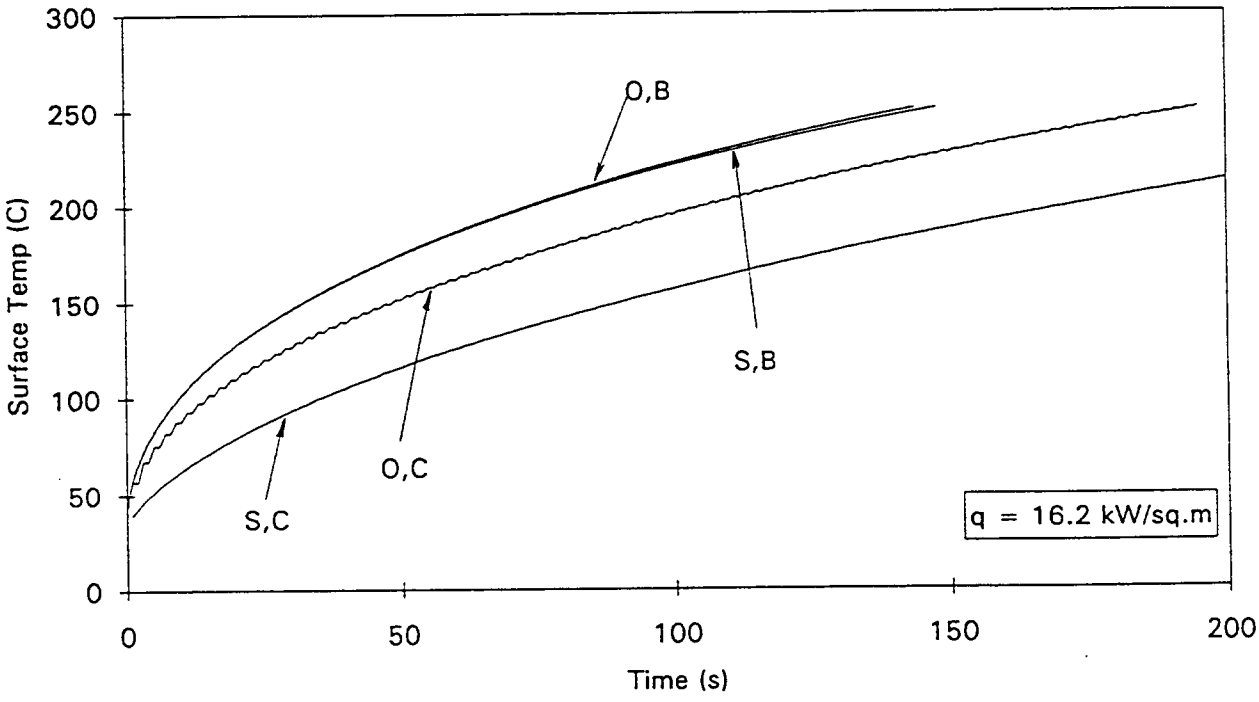

Figure D8: Rise of surface temperature for a PMMA slab. The difference between the clear and the opaque media represents the effect of in-depth absorption. (a) at an external heat flux of 3.7 kW/m^2 and (b) at an external heat flux of 16.2 kW/m^2. O - Opaque medium, S - Semitransparent medium, C - Clear surface, B - Blackened surface

Table 2 - Time required for surface temperature to reach 150 C for samples with clear surface

Flux (kW/m^2)	Time for semitransparent medium (s)	Time for opaque medium (s)	% difference (based on time for opaque medium)
3.7	2332	2130	9.5
6.8	662	513	29.0
12.5	155	95	63.1
16.2	91	49	85.7
23.1	46	19	142.1

values of the heat flux. The temperature rise is extremely sensitive to the heat flux, and a small error in determining the heat flux significantly affects the heat-up time. Second, the model assumes temperature independent properties for PMMA. Nonetheless, the model does predict the same trends as those established in the experiments.

When there is a fire in a confined space, a surface may be subjected to external radiation from surrounding burning walls before actually igniting. However, once combustion has been initiated, the surface is rapidly covered with soot. In the case of semitransparent materials, it will be important to account for in-depth absorption while analyzing heat up time. After ignition, however, the medium can effectively be considered opaque if there is soot deposition.

CONCLUSIONS

An analysis has been carried out to determine the effects of in-depth absorption of externally incident radiation. The radiation model considered the spectral variation of the absorption coefficient obtained from separate experiments. The results from the model were also compared with those obtained from experiments of PMMA. Based on the results for PMMA slabs under external radiation, the following conclusions have been reached.

1. For clear surfaces, the rise of surface temperature is affected by in-depth absorption. Heat- up times are significantly longer for semitransparent media as opposed to opaque media. Upward flame spread on semitransparent media is, therefore, expected to be slower than on opaque media.
2. For a blackened surface, opaque and semitransparent media have nearly the same surface temperature rise. Semitransparent media may thus be considered opaque for upward flame spread purposes when the surface is covered with soot or dust.
3. The radiation problem required the use of a fourteen-band model for PMMA to represent the spectral variation of surface reflectivity and absorption coefficient in order to adequately account for heating under external radiation.
4. The theoretical model demonstrates the same trends as the experiments.

References

Churchill, S. W. and Chu, H. S., 1975, "Correlating equations for laminar and turbulent free convection from a vertical plate," *Int. J. Heat Mass Transfer* **18**, 1323-1329.

Daikoku, M., Venkatesh, S., and Saito, K., 1991, Private communication.

Finlayson E.U., Aung, W., Kashiwagi, T., 1987, "Theoretical models for combined radiation-conduction in polymeric solids heated by external radiative flux," *Proceedings of the 1987 ASME-JSME Thermal Engineering Joint Conference,* Honolulu, Hawaii.

Fernandez-Pello, A. C., 1977, "Upward laminar flame spread under the influence of externally applied thermal radiation," *Comb. Sci. Technol.* **17,** 87-98 .

IMSL (International Mathematical and Statistical Libraries), 1984, 9th ed., GNB Bldg., 7500 Ballaire Blvd., Houston, TX 77036 .

Ito, A., Saito, K., and Inamura, T., 1992, "Holographic interferometry temperature measurements in liquids for pool fires supported on water," *Journal of Heat Transfer*, **114**, 944-949.

Klassen, M., Sivathanu, Y. R., and Gore, J. P., 1992 "Simultaneous emission absorption measurements in toluene-fueled flames: mean and rms properties," *Combust. Flame* **90**, 34-44 .

Kulkarni, A. K., 1990, "Heat feedback in vertical wall fires," *Experimental Heat Transfer* **3,** 411-426.

Manohar, S. S., 1992, "In-depth radiation absorption in semitransparent materials," Master of Science Thesis, Mechanical Engineering, The Pennsylvania State University, University Park, PA.

Myers, V. H., Ono, A., and DeWitt, D. P., 1983, "A new method for measuring optical properties of semitransparent materials at high temperatures," AIAA 18th Thermophysics Conference, Montreal, Canada (1983).

Park, S. H. and Tien, C. L., 1990, "Radiation Induced ignition of solid fuels," *Int. J. Heat Mass Transfer* **33,** 1511-1520.

Saito, K., Williams, F. A., Wichman, I. S., and Quintiere, J. G., 1989, "Upward turbulent flame spread on wood under external radiation,"*J. Heat Transfer* **111,** 438-445.

Siegel, R., and Howell, J. R., 1981, *Thermal Radiation Heat Transfer*. 2nd ed., Hemisphere, New York .

Silverstein, R. M., Bassler, G. C., and Morrill, T. C., 1981, *Spectrometric Identification of Organic Compounds*. 4th ed., Wiley, New York.

Song B. and Viskanta R., 1990, "Deicing of solids using radiant heating," *AIAA Journal of Thermophysics and Heat Transfer* **4**, 311-317.

Tewarson, A. and Ogden, S. D., 1992, "Fire Behavior of Polymethylmethacrylate," *Combustion and Flame*, **89**, 237.

E. REFLECTANCE MEASUREMENTS USING HEATED CAVITY REFLECTOMETER

(In addition to R. B. Nair and A. K. Kulkarni, Professor S. T. Thynell was involved in this project. Dr. Thynell acknowledges the support received from the Office of Naval Research under contract N00014-91-J-4116 with Dr. G.D. Roy serving as the contract monitor.)

Analysis of radiative heat transfer from surfaces requires knowledge of their radiative properties, namely, emissivity, absorptivity and reflectivity. The overall objective of the work presented in this paper is to design and fabricate an apparatus for determining the spectral radiation properties of burnt and nonburning samples of various materials, which are considered for use in studies of flame spread. Additional details on this task may be found in Nair (1993).

Background

The present study carried out experiments to determine the reflectivity for the sample using a heated cavity reflectometer. Gaumer et. al. (1962) used a calorimetric technique to determine thermal radiation characteristics. The calorimetric device consisted of a sample provided with an internal source of energy and suspended within an evacuated chamber with black cryogenic walls. Jansen and Torberg (1963) measured spectral reflectance using an integrating hemisphere. Benford (1934) and Jacquez and Kappenheim (1955) used the integrating sphere reflectometer to carry out measurements of spectral reflectance. The principal feature of their system was a sphere of which the inner surface was totally diffusing and of high reflectance in the spectral region of interest. The heated cavity reflectometer was first developed in 1947 by Gier and Dunkle (1960). An excellent review of some common methods of measuring spectral reflectance and the sources of error inherent in the various techniques is also available in the paper by Dunkle et al. (1962). Gier et al. (1954) measured the absolute spectral reflectivity for different materials using a similar instrument. According to Dunkle (1960), the integrating sphere method is most suitable in the ultraviolet, visible, and near-infrared regions, whereas the blackbody reflectometer is more accurate in the mid- and far-infrared regions. In the present study it was decided to make measurements using the heated cavity reflectometer.

The Apparatus

Overall Design : The reflectometer consists of a cooled sample irradiated over the hemisphere by a surrounding heated cavity. Radiant flux reflected from the sample in a small solid angle is viewed. The directional or angular reflectance is defined here as the ratio of the reflected radiant flux to the flux incident in a differential solid angle $d\Omega$ about a direction given by the polar angle of incidence θ and the azimuthal angle ϕ. The polar angle is measured from the normal to the surface, and the azimuthal angle is measured in the plane of the surface.

The principal components of the heated cavity reflectometer are the aluminum plates which form the casing, the ceramic foam insulation, the heating elements and the sample holder. The reflectometer is used in conjunction with a standard Fourier Transform Infrared (FTIR) spectrometer to determine the reflectance. A cross-section of the assembled reflectometer is shown in Figure E1.

Aluminum Cubical Enclosure : Six aluminum plates, each 0.5" thick, formed the casing of a 13" cubical cavity. One inch diameter holes were drilled in the aluminum plates for insertion of the sample holder and burner rod, and for the removal of combustion gases, and for a view port to the FTIR. Copper tubes were soldered to aluminum angle strips using a special kind of alloy solder. The angle strips were then screwed into the aluminum plates. Water flowing through the tubes ensured that the aluminum plates remained cool.

Ceramic Foam and Blanket : The ceramic foam was in the form of solid blocks of 9" x 9" x 3". These were easily machineable and can withstand temperatures up to 3300 F. The blocks were cut into appropriate shapes so that a uniform insulation thickness of 3" was obtained inside the aluminum casing, thus forming a cubical cavity of length 7 inches. Holes of one inch diameter aligned with those in the aluminum plates were drilled through the foam blocks. The ceramic blanket was inserted in between the foam blocks and the aluminum casing to ensure better insulation and a tight fit.

Heating Elements and Power Control : The flat-plate type heating elements had heating (nichrome) wire running through a ceramic base. These were 7" x 2.75" x 0.4" thick and each had a maximum power rating of 240 W, 57.5 volts. Two heaters were mounted on each face of the cubical cavity formed by the ceramic foam blocks. Ceramic glue was used to fix the heating elements flush with the walls forming the cavity. The power input to each heater was

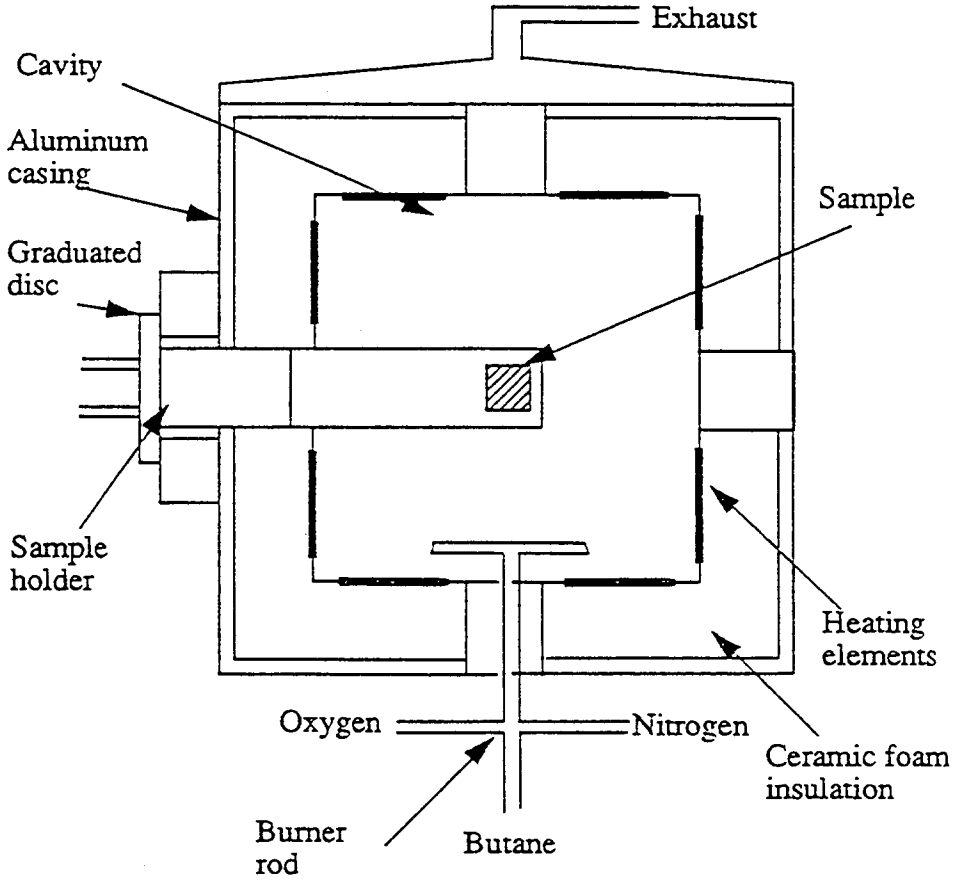

Figure E1:. Heated Cavity Reflectometer Cross-section

controlled by a variac, so that individual regulation of the heating elements was possible. This was later helpful in making minor adjustments so that a reasonably isothermal cavity was obtained.

Sample Holder : The sample holder was fabricated out of a one inch diameter, 9" long solid aluminum cylinder. Figure E2 shows a detailed view of the sample holder. The part of the sample holder that would protrude into the cavity was cut to be a hemispherical cylinder. The sample was mounted on the flat face of the sample holder using a highly conducting thermal paste. Two holes of diameter 0.125" carrying cooling water were drilled through the length of the holder. Another hole through the sample holder was drilled for insertion of a thermocouple to measure temperature of the sample. Threads were cut on one end of the sample holder and a retaining nut was screwed into place. This along with a collar made sure that the sample holder was fixed in position when a reading was taken. A graduated disc (in degrees) was attached to the collar, so that the sample holder could be rotated through a desired angle (polar angle of measurement).

Temperature Measurement : K-type (chromel-alumel) thermocouples were inserted through holes drilled in the ceramic foam blocks, and were positioned so that they were flush against the cavity wall. Ceramic paste was used to fix the thermocouples firmly in place. This ensured that the temperature read by the thermocouple was that of the surface of the wall. Two thermocouples were used for each face of the cavity to further reduce possible error. Since it was desired that the reflectometer could be operated at temperatures of more than 1000 K, the thermocouples had a ceramic fiber insulation sheath as a safeguard.

FTIR Spectrometer : A standard FTIR was used to determine the reflectance of the samples. The wavelength range from 0.67 to 20 m was covered using a combination of detectors. An Si detector from 0.67 to 1.1 m, a lead selenide detector from 1 to 2.5 m, and a MCT detector from 2 to 20 m along with a either a Ge coated on KBr substrate or a quartz beam splitter were used. Thereby, wavelengths from near to far infrared could be detected. The FTIR generated a modulated beam by splitting the infrared beam from the cavity into two parts, one of which was reflected onto a stationary mirror and the other onto a mirror which was moving at a constant speed. The two beams were subsequently recombined to form a modulated beam. Details of FTIR operation and IR spectroscopy can be obtained from Coleman et al. (1987).

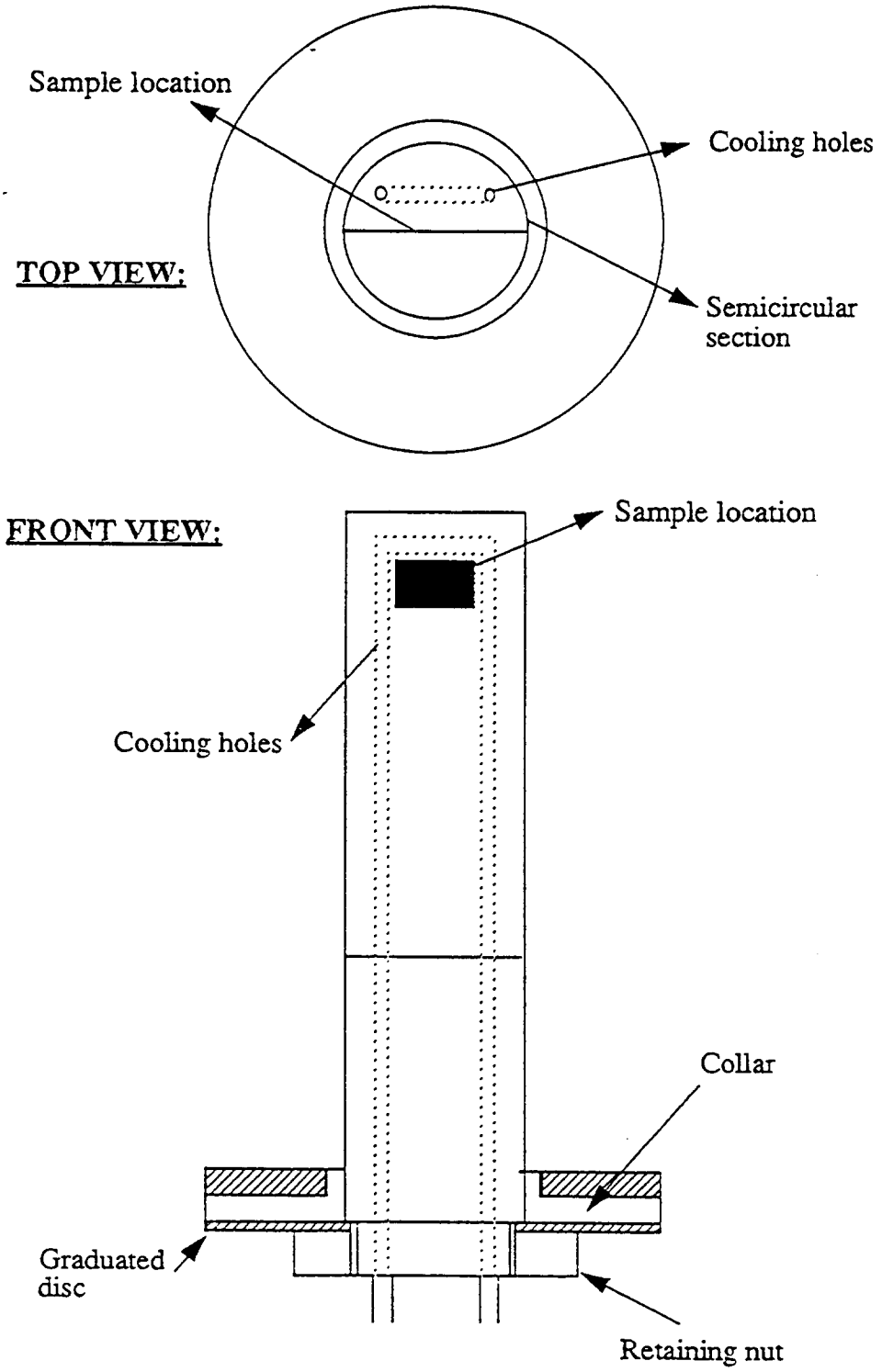

Figure E2: Detailed view of sample holder

Assembly : The heating elements were first fixed to the ceramic foam blocks, two to a side, using the ceramic glue, and they were cured in a furnace at 800 degrees C for 3-4 hours. The thermocouples were then fixed to the cavity wall surface. The aluminum casing was then bolted into place, after inserting the ceramic blanket between the casing and the foam blocks. The thermocouples were taken out through the back face of the reflectometer. The heater leads were taken out from the top and the front face. To ensure that there was no contact between the live heating wire and the aluminum plate, a hard ceramic sheath was inserted over the lead wire thus insulating it from contact with the aluminum. The ends of the lead wire were then attached to binding posts which were fixed tightly to the aluminum plate. The power supply to the heating elements was controlled by variacs. Each of the twelve heaters had its own variac, which was mounted on a panel along with the fuse box. The variacs were rated at 120 V, 1.20 kVA and the fuses at 4 amperes. The fuse was in line with the heating elements. Thermocouples were attached to a digital display v. selector switch. The identity of the thermocouples on each face of the cavity was carefully noted, whereby depending on the nonuniformity in the temperature of the cavity, the corresponding wall temperature could either be raised or lowered by adjusting the variac. The reflectometer was placed on a stand which could be raised or lowered using leveling screws, so that the viewing port of the reflectometer could be aligned with the FTIR.

Experiments

In the present work, measurements of angular reflectance were made for non-burning samples only. Six different samples (gold, aluminum, clear and black PMMA, polycarbonate, and paper) were used. Figure E3 shows a schematic of the experimental setup. Before startup of the reflectometer, a background emission reading was taken. The alignment of the sample with respect to the exit port was checked with the laser beam from the FTIR. Two strips of aluminum were pasted onto the exit port with a very small gap between them. This was done so that the detector would measure only the energy from the very small aperture formed. Alignment of the sample was accomplished when the focus of the laser beam remained in the center of the sample as it was rotated from 0 to 90 degrees. A retaining nut and a strip of aluminum ensured that the sample holder was held fixed at each angular position while the measurement was in progress. The zero error in the setting of the graduated disc with respect to the sample was noted. Power to the heaters was then switched on. The variacs were used to set the voltage to obtain a desired steady- state temperature. The cooling water was turned on

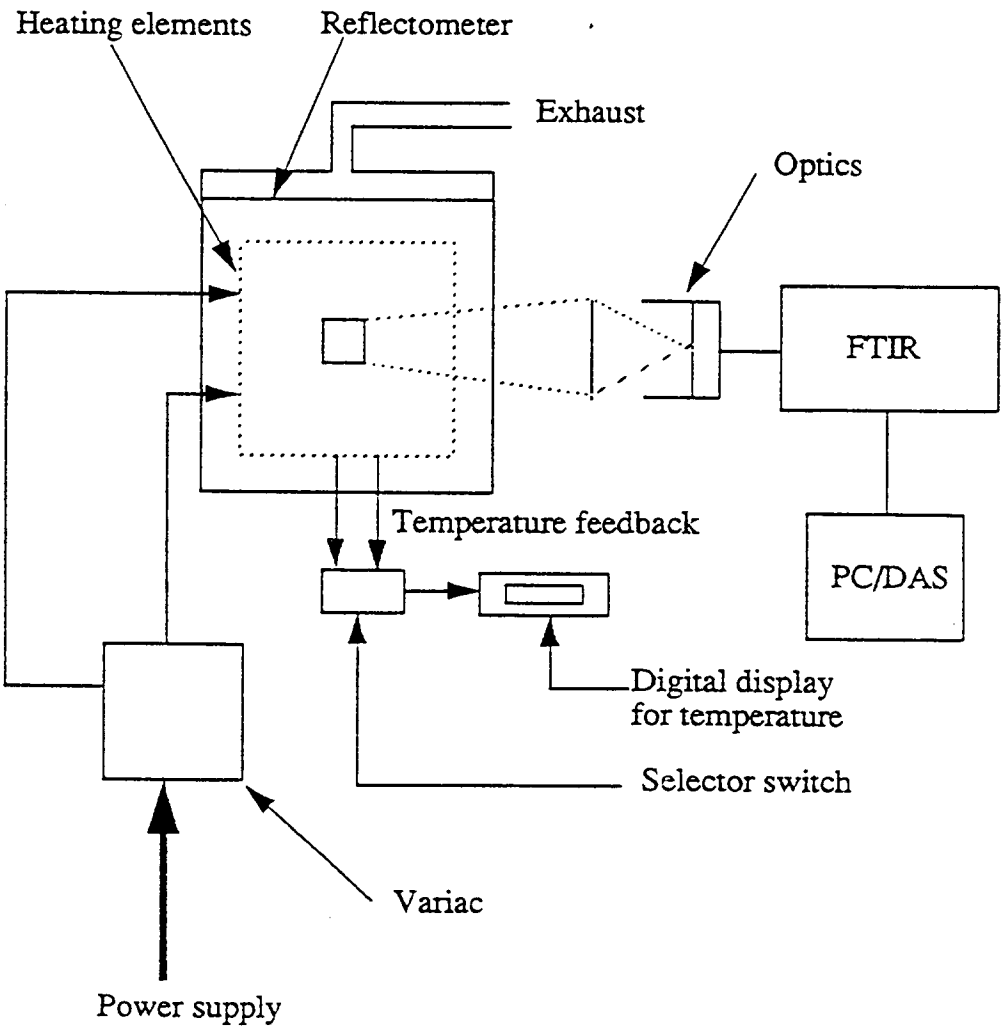

Figure E3: Schematic of Heated Cavity Reflectometer Setup

so that the aluminum casing would not heat up. About two hours were necessary for the furnace to reach a steady state temperature of about 650 degrees C.

Thermocouples at various positions in the cavity could be monitored for slight differences in temperature by using the selector switch and the digital display. Adjusting the respective variac, and thereby changing the power input to the heater, the temperature of the cavity could be adjusted manually to minimize the observed differences. Once at the desired steady temperature, a reading for emission from the cavity was taken. Since the radiation detected by the FTIR was from a very small aperture compared to the size of the cavity, the radiation from the cavity could be approximated by that from a blackbody at the same steady state temperature.

Next, the sample (0.75" x 0.75") was pasted on to the sample holder using a highly conducting thermal paste. Readings were taken at intervals of 5 degrees from 0 degrees to 90 degrees. The reflectometer was first characterized by using a gold plated quartz sample. Since the sample was quite thick, and there was a danger of the sample sliding off into the furnace, only angles from 0 to 60 degrees were considered. Also, because of the thickness of the sample, it was impossible to ensure that it remained at a very low temperature and would not heat up for the duration of the measurement. Hence, after every angular setting, the sample holder was removed, and the sample was allowed to cool. Samples of aluminum, clear PMMA, black PMMA, polycarbonate and paper were also tested. Since the aluminum and paper samples were very thin, and the sample holder was quite efficiently cooled, the samples never reached temperatures at which emission from the sample itself would be significant. Therefore, it was possible to take measurements at all angular settings without removing the sample holder from the cavity However, for polycarbonate and both types of PMMA, this was not possible. In fact, the sample itself had to be changed for every angular setting because the temperature of the sample increased rapidly thereby causing changes in the structure of the material. Results of the measurements of surface reflectivity for the different samples are presented in the next section.

Results and Discussion

The output was obtained by a PC based data acquisition system (DAS) inter-faced with the FTIR. Since there was significant noise in the signal from the FTIR near the limits of the measuring range of the detector, the data points near the two limits were discarded. The set of conditions at which the experiments were conducted are shown below.

Average wall temperature	~650 C
Average heater voltage	~30 volts
FTIR detector temperature	70 K

To get the relative spectral directional reflectance ($\rho_{\theta\nu}$) of the sample, the background emission signal (S_{be}), was subtracted from the reflected signal (S_r), and the black body emission signal (S_e). The ratio of the reflected signal to the black body signal gave the relative directional reflectance

$$\rho_{\theta\nu} = \frac{S_r - S_{be}}{S_e - S_{be}}$$

A small computer program was written in order to read the data file generated by the data acquisition system, and convert it to the proper format for plotting. The output from the DAS consisted of spectral reflectance at different wavenumbers. Besides putting in the proper format to plot the reflectance versus wavenumbers, the program also integrated the spectral reflectance over the desired wavenumber range to obtain the total directional reflectance, ρ_θ, using

$$\rho_\theta = \frac{\int_{\nu_1}^{\nu_2} \rho_{\theta\nu} E_{b\nu}(T) d\nu}{\int_{\nu_1}^{\nu_2} E_{b\nu}(T) d\nu}$$

where ν_1 and ν_2 are the limits of the desired wavenumber range. Plots for directional reflectance as a function of the polar angle and for spectral normal reflectance as a function of wavenumber for the six different samples are shown in figures E4 through E16. Figures E4 and E5 show the relative directional reflectivity and the spectral normal reflectivity for gold. A sharp dip is seen at a polar angle of 45 degrees. This is probably due to the nonuniformity in the cavity-wall temperature. The reflectivity does not vary widely with the polar angle, however, showing that gold is relatively diffuse. For very high wavenumbers, the normal reflectivity shows substantial noise because the signal to noise ratio is quite low in this region. For wavenumbers less than 5000 cm-1, the plot is quite flat, showing that it is relatively independent of wavenumber. The plots for aluminum exhibit similar behavior

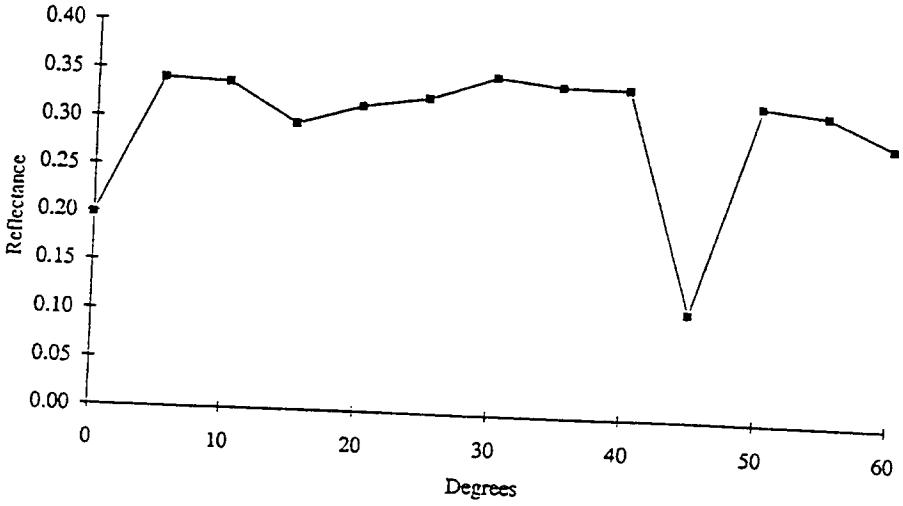

Figure E4: Relative directional reflectance of gold

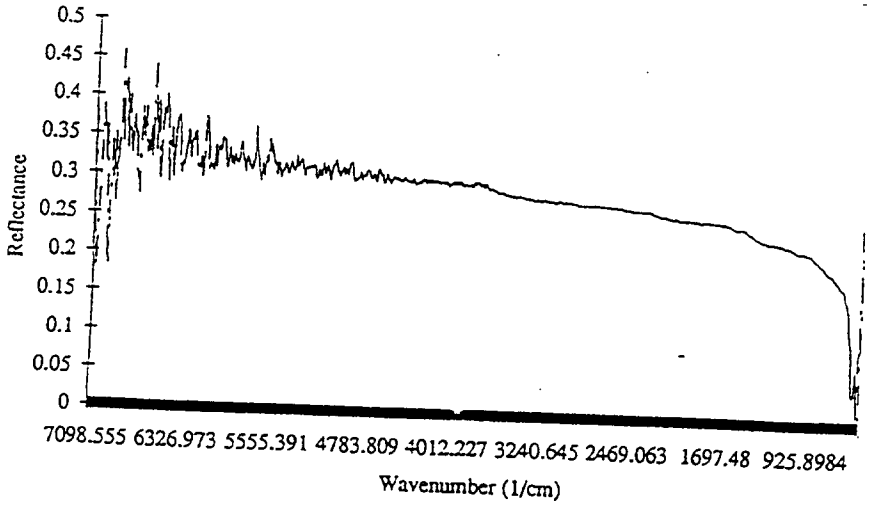

Figure E5: Spectral normal reflectance of gold

indicating that aluminum is relatively diffuse (Figures E6 and E7). The sharp dip at 45 degrees occurred for the same reasons as previously described for gold. However, the reflectivity for aluminum is lower than that for gold. The variation of normal reflectivity with wavenumber again shows a low signal to noise ratio for higher wavenumbers, while remaining relatively flat for lower wavenumbers. Paper (Figures E8 and E9) and polycarbonate (Figures E10 and E11) were relatively diffuse, with not much change in the reflectivity as the polar angle was changed from 0 to 90 degrees. For paper, the directional reflectivity shows a steady increase with the polar angle, peaks very near 90 degrees and then drops suddenly. The plot for the spectral normal reflectance reveals many peaks and valleys. This happens because of the complex molecular nature of paper, which consists of nitrocellulose. The peaks and valleys in the plot could be attributed to the complex organic compounds that can be found in the structure of paper. However, it is not possible at this stage to reveal the finer details of the structure by looking at the graph of spectral normal reflectance. Again, for higher wavenumbers, the signal to noise ratio is quite low, so the reflectance values show very sharp fluctuations.

Polycarbonate shows a similar behavior as paper for the directional reflectance, indicating a slow increase with the polar angle, peaking at values close to 90 degrees. The graphs for clear PMMA (Figures E12, E13 and E14) show that for most of the wavenumbers, the material is quite black. The reflectance values are small, except at very low wavenumbers. For higher wavenumbers, the low signal to noise ratio again comes into play. Clear PMMA also shows a reasonably diffuse behavior except very near 90 degrees. The data obtained from the current study is compared to the results from Manohar (1992). Reflectance values for black PMMA are considerably lower than for clear PMMA (Figures E15 and E16). The spectral reflectance plot shows that the material is quite black for a wide range of wavenumbers, which comes as no surprise. There is a slight increase, though, for smaller wavenumbers. The zigzag nature of the directional reflectance plot could be due to the effect of noise in the results.

A discussion of some of the errors inherent in using the heated cavity reflectometer can be found in Gaumer et. al. (1962), Dunkle (1960) and Modest (1992). If the sample gets heated, then emission from the sample is a major source of error. This error is proportional to the spectral emittance of the sample. However, the sample temperature was measured and found to remain quite low compared to the cavity temperature, and thereby, it is assumed that there was negligible emission. Besides, in the case of metallic samples, the surface properties

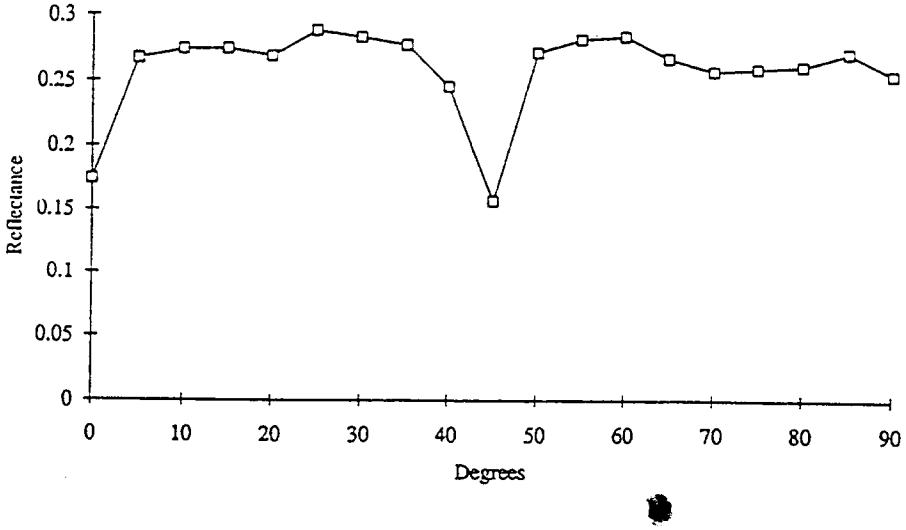

Figure E6: Relative directional reflectance of aluminum

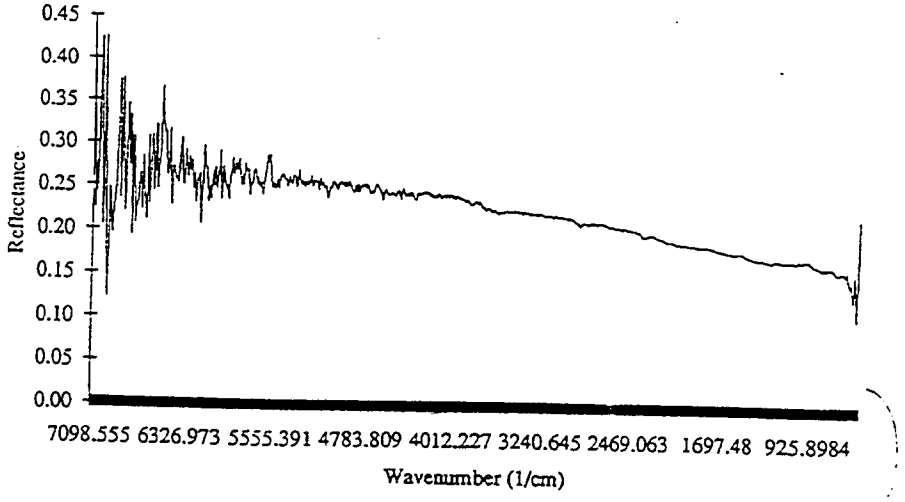

Figure E7: Spectral normal reflectance of aluminum

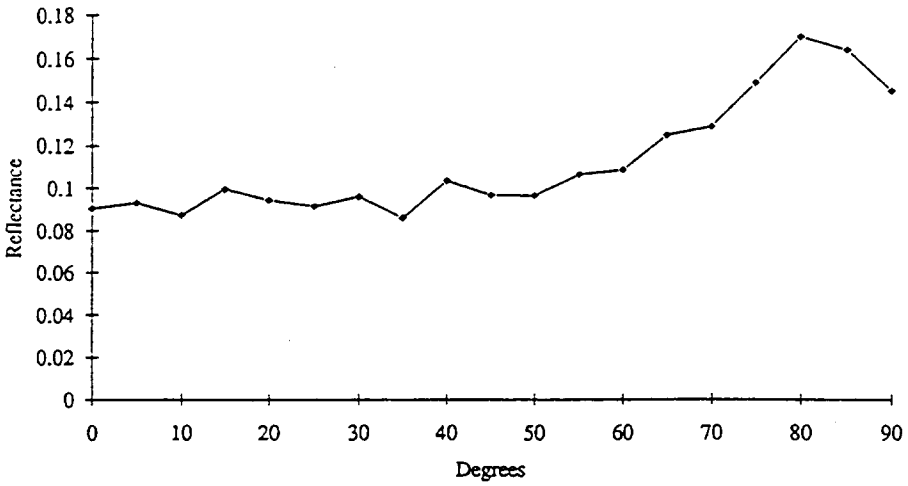

Figure E8: Relative directional reflectance of paper

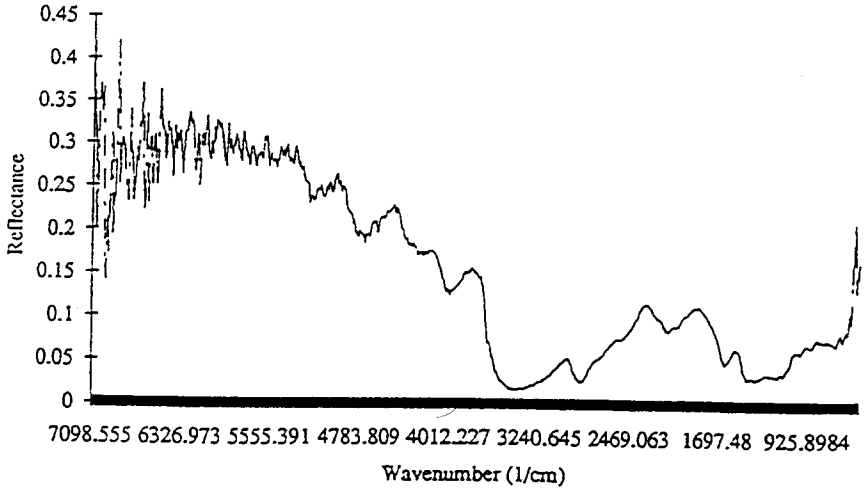

Figure E9: Spectral normal reflectance of paper

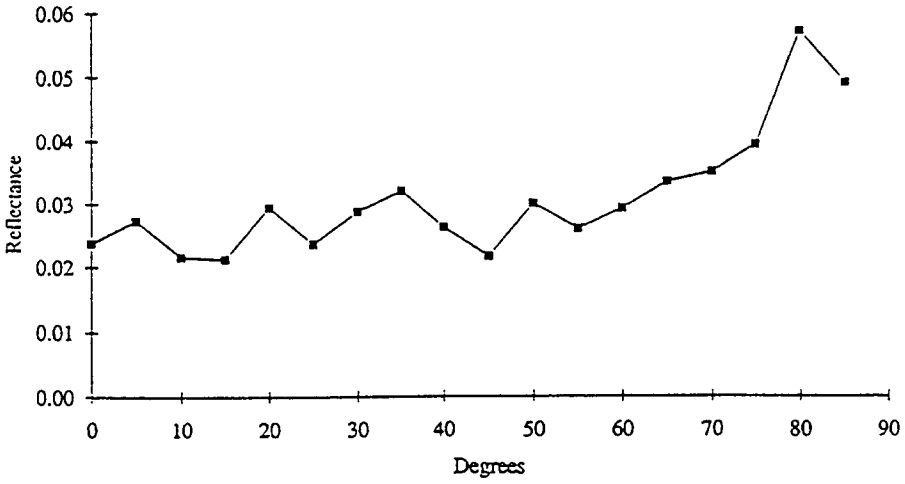

Figure E10: Relative directional reflectance of polycarbonate

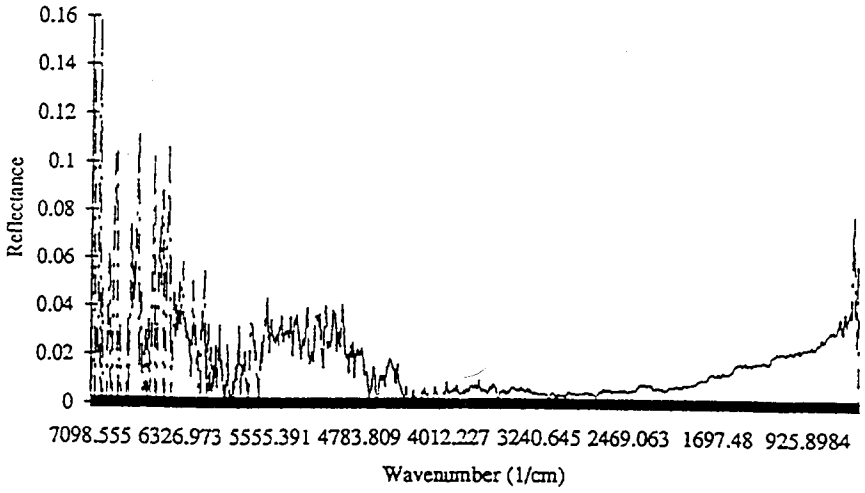

Figure E11: Spectral normal reflectance of polycarbonate

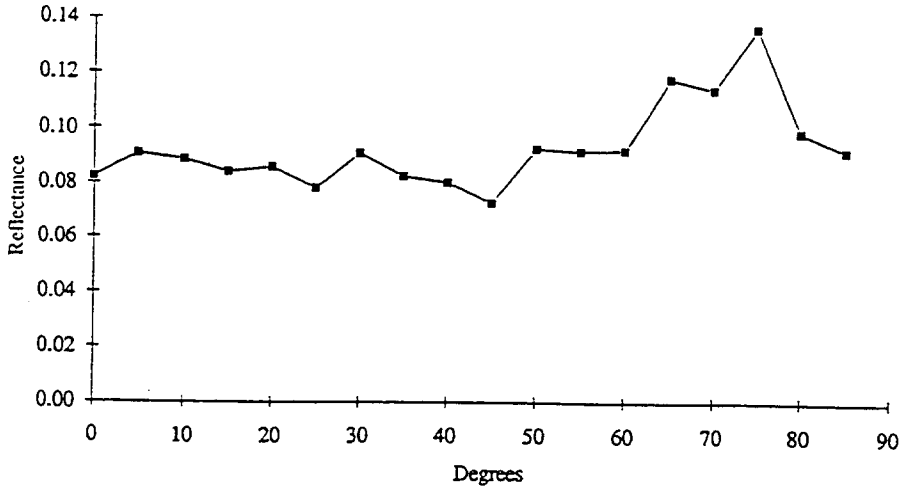

Figure E12: Relative directional reflectance of PMMA

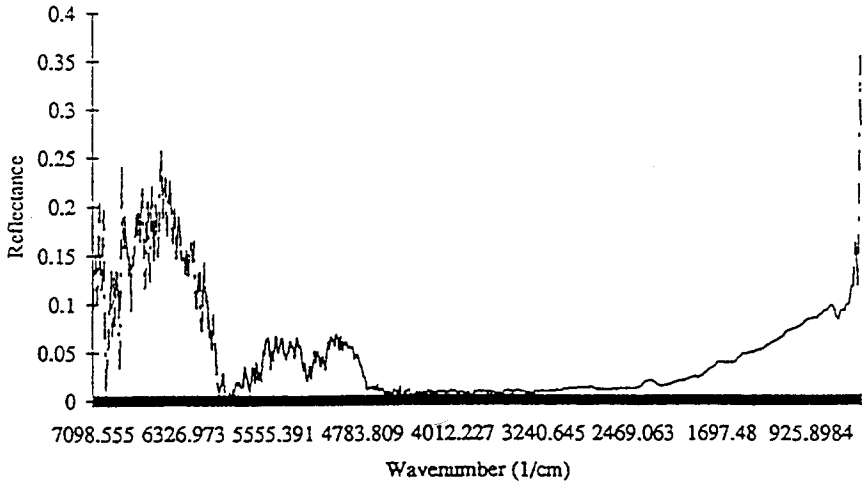

Figure E13: Spectral normal reflectance of PMMA

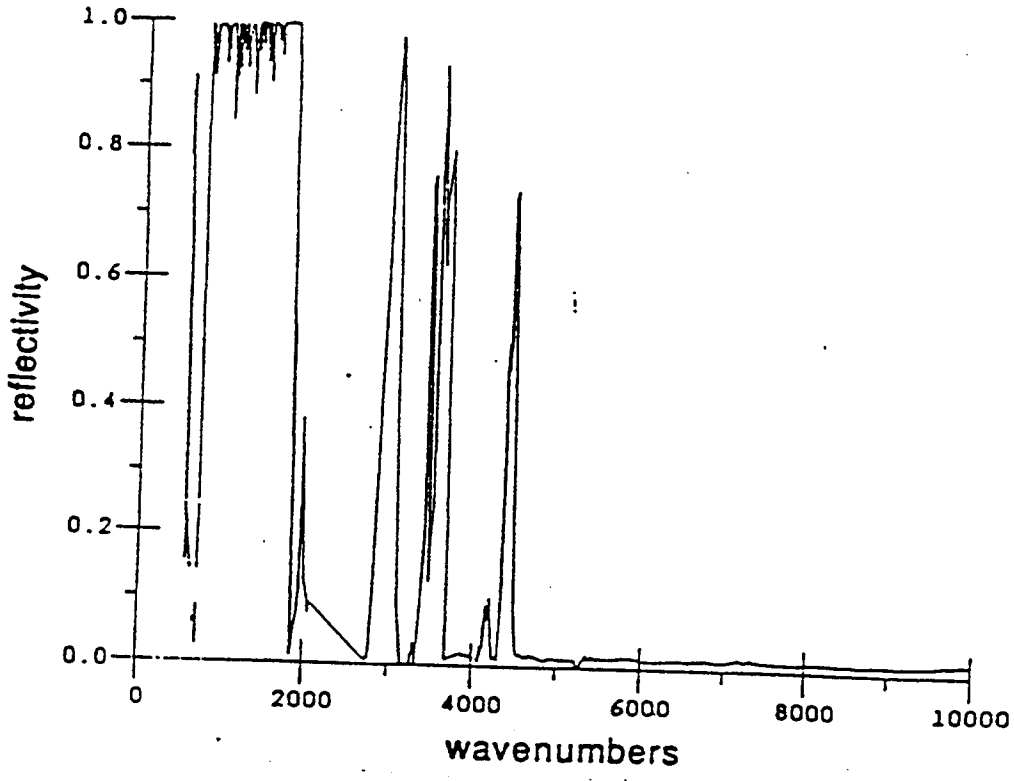

Figure E14: Spectral normal reflectance of PMMA [10]

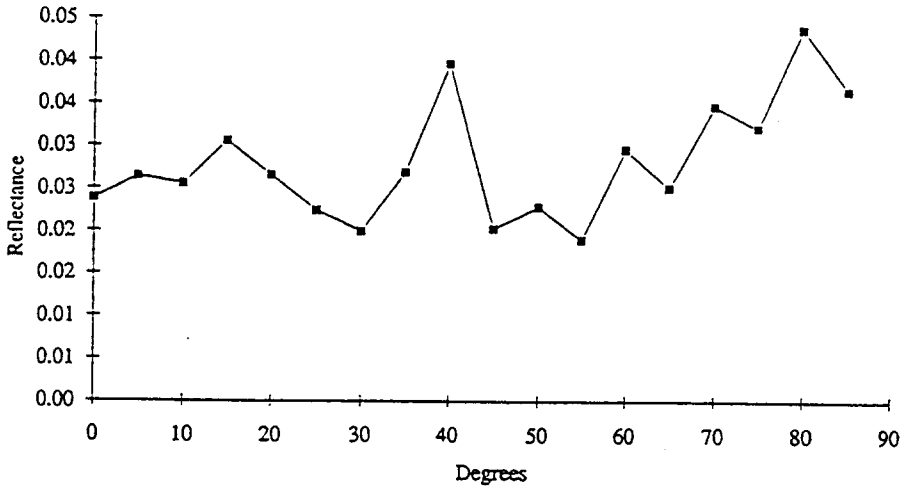

Figure E15: Relative directional reflectance of black PMMA

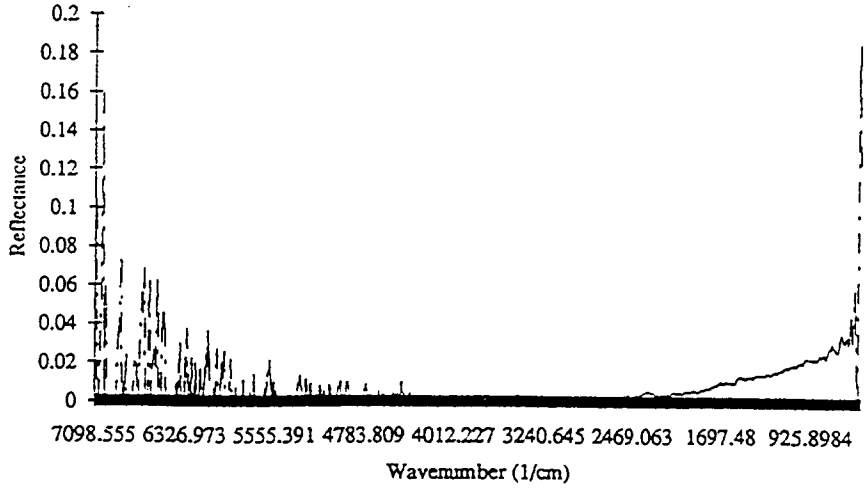

Figure E16: Spectral normal reflectance of black PMMA

might change due to formation of an oxide film, or in the case of nonmetallic substances like PMMA, changes is structure might occur which would cause it to behave as an entirely different material. A second error arises due to nonuniformities in the cavity wall temperature. Since there is a practical necessity for apertures in any enclosure used to irradiate the sample, this necessarily invalidates the assumption of uniformity in the cavity wall temperature. However, temperature differences were kept to a minimum by adjusting the variacs for the respective heaters, so that the energy emitted by the cavity and seen by the reflectometer closely approximates black body radiation at the desired uniform temperature.

Summary and Conclusions

A heated cavity reflectometer that can be used to carry out directional measurements of reflectance in the 1.5 micron to 20 micron range was designed and fabricated. Spectral normal and total directional reflectance for six different samples were measured. The reflectometer has also been designed to measure reflectivity for burning materials. However, these experiments have not been carried out yet. In order to carry out such work using an FTIR, care will have to be taken to isolate absorption spectra due to products of combustion like carbon dioxide, and/or other organic gases which might be released during burning or materials like PMMA or polycarbonate. The desired result is to obtain spectra due to the reflected energy from the sample and the effects of selective absorption due to combustion gases must be taken into account. Obtaining measurements of burning sample surfaces will be of great help in improving our understanding of flame spread, and be of use in predictive models of such phenomena.

References

Benford, F., 1934, "A Reflectometer for All Types of Surfaces", *Journal of the Optical Society of America,* vol. 24, p.165.

Coleman, M. M., and Painter, P. C., 1987, "Infrared Absorption Spectroscopy", *Encyclopedia of Polymer Science and Engineering*, John Wiley and Sons, Inc., vol. 8, p. 69.

Dunkle, R. V.,1960, "Spectral Reflectance Measurements", *Surface Effects on Spacecraft Materials*, edited by F. J. Clauss, John Wiley and Sons, Inc., New York, pp. 117-137.

Dunkle, R. V., Edwards, D. K., Gier, J. T., Nelson, K. E., and Roddick, R. D., 1962, "Heated Cavity Reflectometer for Angular Reflectance Measurements", *Progress in International Research on Thermodynamic and Transport Properties*, American Society of Mechanical Engineers., New York, pp. 541-562.

Gaumer, R. E., Mckellar, L. A., Streed, E. R., Frame, K. L., and J. R. Grammer, 1962, "Calorimetric determination of Thermal Radiation Characteristics", *Progress in International Research on Thermodynamic and Transport Properties*, American Society of Mechanical Engineers, New York, pp. 575-587.

Gier, J. T., Dunkle, R. V., and Bevans, J. T., 1954, "Measurement of Absolute Spectral Reflectivity from 1.0 to 15.0 Microns", *Journal of the Optical Society of America*, vol.44, pp. 558-562.

Jacquez, J. and Kappenheim, H., 1955, "Theory of the Integrating Sphere", *Journal of the Optical Society of America,* vol. 45, nos. 6 and 11.

Janssen, J. E., and R. H. Torberg, 1963, "Measurement of Spectral Reflectance Using an Integrating Hemisphere", *Measurement of Thermal Radiation Properties of Solids,* NASA-SP-31, pp. 169-182.

Manohar, S. S., 1992, "In-depth Radiation Absorption in Semitransparent Materials", M.S. Thesis, The Pennsylvania State University.

Modest. M., F., 1992, *Radiative Heat Transfer*, McGraw Hill Publishing Co.

Nair, R., 1993 Measurement of Spectral Hemispherical Reflectance Using a Heated Cavity Reflectometer, M. S. Thesis, The Pennsylvania State University.

NIST-114
(REV. 9-92)
ADMAN 4.09

U.S. DEPARTMENT OF COMMERCE
NATIONAL INSTITUTE OF STANDARDS AND TECHNOLOGY

MANUSCRIPT REVIEW AND APPROVAL

(ERB USE ONLY)
ERB CONTROL NUMBER | DIVISION
PUBLICATION REPORT NUMBER: NIST-GCR-93-638 | CATEGORY CODE
PUBLICATION DATE: June 1994 | NUMBER PRINTED PAGES

INSTRUCTIONS: ATTACH ORIGINAL OF THIS FORM TO ONE (1) COPY OF MANUSCRIPT AND SEND TO: THE SECRETARY, APPROPRIATE EDITORIAL REVIEW BOARD.

TITLE AND SUBTITLE (CITE IN FULL)

Turbulent Upward Flame Spread on a Vertical Wall Under External Radiation

CONTRACT OR GRANT NUMBER
Grant No. 60NANB8D0849

TYPE OF REPORT AND/OR PERIOD COVERED
Annual Report
September 30, 1991 - January 15, 1993

AUTHOR(S) (LAST NAME, FIRST INITIAL, SECOND INITIAL)
A.K. Kulkarni, E. Brehob, S. Manohar, R. Nair
Pennsylvania State University
University Park, PA 16802

PERFORMING ORGANIZATION (CHECK (X) ONE BOX)
[ ] NIST/GAITHERSBURG
[ ] NIST/BOULDER
[ ] JILA/BOULDER

LABORATORY AND DIVISION NAMES (FIRST NIST AUTHOR ONLY)

SPONSORING ORGANIZATION NAME AND COMPLETE ADDRESS (STREET, CITY, STATE, ZIP)
U.S. Department of Commerce
National Institute of Standards and Technology
Gaithersburg, MD 20899

RECOMMENDED FOR NIST PUBLICATION

[ ]	JOURNAL OF RESEARCH (NIST JRES)	[ ]	MONOGRAPH (NIST MN)	[ ]	LETTER CIRCULAR
[ ]	J. PHYS. & CHEM. REF. DATA (JPCRD)	[ ]	NATL. STD. REF. DATA SERIES (NIST NSRDS)	[ ]	BUILDING SCIENCE SERIES
[ ]	HANDBOOK (NIST HB)	[ ]	FEDERAL INF. PROCESS. STDS. (NIST FIPS)	[ ]	PRODUCT STANDARDS
[ ]	SPECIAL PUBLICATION (NIST SP)	[ ]	LIST OF PUBLICATIONS (NIST LP)	[X]	OTHER NIST-GCR
[ ]	TECHNICAL NOTE (NIST TN)	[ ]	NIST INTERAGENCY/INTERNAL REPORT (NISTIR)		

RECOMMENDED FOR NON-NIST PUBLICATION (CITE FULLY) [ ] U.S. [ ] FOREIGN

PUBLISHING MEDIUM
[ ] PAPER [ ] CD-ROM
[ ] DISKETTE (SPECIFY)
[ ] OTHER (SPECIFY)

SUPPLEMENTARY NOTES

ABSTRACT (A 1500-CHARACTER OR LESS FACTUAL SUMMARY OF MOST SIGNIFICANT INFORMATION. IF DOCUMENT INCLUDES A SIGNIFICANT BIBLIOGRAPHY OR LITERATURE SURVEY, CITE IT HERE. SPELL OUT ACRONYMS ON FIRST REFERENCE.) (CONTINUE ON SEPARATE PAGE, IF NECESSARY.)

Progress made on NIST grant number 60NANB8D0849 for the period September 30, 1991 to January 15, 1993 is reported. The overall objective is to understand the upward flame spread phenomenon under simulated surrounding fire conditions by establishing a data base for upward flame spread under external radiation, developing a mathematical model, measuring the relevant basic material properties needed, and checking the validity of the model by comparing its results with data. Emphasis is placed on studying and predicting the behavior of practical wall materials used in building and vehicle interiors, and textiles. In the past year, we measured flame spread on several different materials under a range of external radiant fluxes of up to 15 kW/m^2. A model for describing the upward flame spread process was developed and numerical results were compared with data. The model needed input of certain properties, such as the burning rate characteristics and surface radiation properties. A series of supporting studies were undertaken which provided the needed input properties to the model and other useful material property data.

KEY WORDS (MAXIMUM 9 KEY WORDS; 28 CHARACTERS AND SPACES EACH; ALPHABETICAL ORDER; CAPITALIZE ONLY PROPER NAMES)

building fires; fire research; flame spread; interior linings; mathematical models; radiation; transportation; vehicles; wall coverings; walls

AVAILABILITY
[X] UNLIMITED
[ ] FOR OFFICIAL DISTRIBUTION. DO NOT RELEASE TO NTIS.
[ ] ORDER FROM SUPERINTENDENT OF DOCUMENTS, U.S. GPO, WASHINGTON, D.C. 20402
[X] ORDER FROM NTIS, SPRINGFIELD, VA 22161

NOTE TO AUTHOR(S) IF YOU DO NOT WISH THIS MANUSCRIPT ANNOUNCED BEFORE PUBLICATION, PLEASE CHECK HERE. [ ]

ELECTRONIC FORM